The Cyclophilin CYP20-2 Modulates the Conformation of BRASSINAZOLE-RESISTANT1, Which Binds the Promoter of *FLOWERING LOCUS D* to Regulate Flowering in *Arabidopsis*[W][OPEN]

Yuanyuan Zhang,[a,b,1] Beibei Li,[a,1] Yunyuan Xu,[a] Heng Li,[c] Shanshan Li,[c] Dajian Zhang,[a,b] Zhiwei Mao,[a] Siyi Guo,[a] Chunhong Yang,[d] Yuxiang Weng,[c] and Kang Chong[a,2]

[a] Key Laboratory of Plant Molecular Physiology, Institute of Botany, Chinese Academy of Sciences, Beijing 100093, China
[b] University of Chinese Academy of Sciences, Beijing 100049, China
[c] Laboratory of Soft Matter Physics, Institute of Physics, Chinese Academy of Sciences, Beijing 100190, China
[d] Key Laboratory of Photobiology, Institute of Botany, Chinese Academy of Sciences, Beijing 100093, China

ORCID ID: 0000-0003-4364-778x (K.C.).

Brassinosteroids (BRs) regulate many physiological processes during plant development, including flowering. However, little is known about the components of BR signaling that mediate flowering. Here, we report that BRASSINAZOLE-RESISTANT1 (BZR1), the conformation of which is altered by a cyclophilin (CYP20-2), binds *cis*-elements in the *FLOWERING LOCUS D* (*FLD*) promoter to regulate flowering. Both *bzr1-1D* and *fld-4* showed delayed flowering. Electrophoretic mobility shift assay and chromatin immunoprecipitation revealed that BZR1 bound to a putative BR response *cis*-element and suppressed the expression of *FLD*. Overexpression of *FLD* partially rescued the late flowering of *pBZR1:mBZR1^Pro234-Leu^-CFP* (mx3). Yeast two-hybrid and pull-down assays demonstrated that BZR1 interacts with CYP20-2. *Arabidopsis thaliana* CYP20-2 had greater peptidyl-prolyl *cis-trans* isomerase activity than did wheat (*Triticum aestivum*) CYP20-2. Fourier transform infrared spectroscopy revealed conformation changes in BZR1, dependent on interaction with CYP20-2. Due to differences in activity and substrate preference between CYP20-2 proteins from wheat and *Arabidopsis*, At-*CYP20-2*–overexpressing lines showed earlier flowering, whereas Ta *CYP20-2* lines flowered later. Immunoblot and chromatin immunoprecipitation assays showed that histone H3 trimethyl Lys4 and H3 acetylation levels were negatively correlated with the transcription of *FLD* (a putative histone demethylase) in various lines. Therefore, a conformational change of BZR1 mediated by CYP20-2 causes altered flowering through modulation of *FLD* expression.

INTRODUCTION

Flowering is a major developmental process that initiates the transition from vegetative to reproductive growth in plants. The genetic network mediating flowering is subject to epigenetic regulation and consists of the photoperiod, vernalization, gibberellin (GA), and autonomous pathways. A key component in the autonomous pathway is *FLOWERING LOCUS C* (*FLC*), a MADS (for yeast MCM1, plant AGAMOUS and DEFICIENS, and mammal Serum Response Factor) box transcriptional repressor (Rouse et al., 2002). FLC binds and represses floral-promoting genes, such as *SUPPRESSOR OF OVEREXPRESSION OF CONSTANS1* (*SOC1*) (Searle et al., 2006). Targeted 3′ processing of antisense *FLC* transcripts triggers chromatin silencing to regulate flowering in *Arabidopsis thaliana* (Liu et al., 2010). Specifically, *FLC* expression is mediated by Lys and Arg histone modifications

(Wang et al., 2007). For example, PROTEIN ARGININE METHYL-TRANSFERASE5 (PRMT5)/Shk1 KINASE BINDING PROTEIN1 (SKB1), mediating Arg methylation of histone, is essential for proper pre-mRNA splicing, especially of *FLOWERING LOCUS K* (*FLK*). In *prmt5* mutants, functional *FLK* transcript and protein levels are reduced, leading to upregulated *FLC* and delayed flowering (Deng et al., 2010). *SET DOMAIN GROUP25* (*SDG25*) encodes a histone methyltransferase, and the loss-of-function mutant *sdg25-1* confers early flowering associated with suppression of *FLC* expression (Berr et al., 2009). In addition, *FLOWERING LOCUS D* (*FLD*), a plant homolog of the human protein *LYSINE-SPECIFIC HISTONE DEMETHYLASE1* (*LSD1*), represses *FLC* expression via histone modification (He et al., 2003; Shi et al., 2004). However, little is known about how *FLD* is regulated.

Brassinosteroids (BRs) regulate multiple processes, including photomorphogenesis and organogenesis, as well as flowering in plants (Bai et al., 2007; Wang et al., 2008; Li et al., 2010b). BR signaling targets the flowering genetic network through two nodes, brassinosteroid insensitive 1 (BRI1) and BRI1-EMS-suppressor 1 (BES1; Domagalska et al., 2007; Yu et al., 2008). BRI1 and BAK1 coperceive BRs at the plasma membrane (Clouse et al., 1996). BSKs mediate signal transduction from the receptor kinase BRI1 to BSU1, which triggers BIN2, a glycogen synthesis kinase 3–like protein (Tang et al., 2008). The *bri1* mutants exhibit late flowering, and those null alleles show very strong late flowering phenotypes.

The double mutants *bri1 fca* and *bri1 fri* have elevated expression of *FLC* and a more severe flowering phenotype (Domagalska et al., 2007).

The basic helix-loop-helix (bHLH) transcription factors BRAS-SINAZOLE RESISTANT1 (BZR1) and BRI1 EMS SUPPRESSOR1 (BES1/BZR2) are positive regulators of BR signaling with dual roles in activating BR responses and negative feedback on BR biosynthesis (Wang et al., 2002; Yin et al., 2002). BZR1 and BES1 are functionally regulated by phosphorylation. Degradation of BZR1 via 26S proteasome–mediated proteolysis requires BIN2-mediated phosphorylation (He et al., 2002; Jin et al., 2006). Phosphorylation-dependent nucleocytoplasmic shuttling of BES1 is important for regulating BR signaling output (Ryu et al., 2010b). BSU1 and BIN2 are required for cellular spatial redistribution of phosphorylation-dependent BES1 in BR signaling (Ryu et al., 2010a). The phosphatase PP2A dephosphorylates BZR1 to affect BR signaling (Li and Jin, 2007; Ryu et al., 2007; Tang et al., 2011). In addition, BZR1 signaling is balanced by the transcription factor LIC, a turn-off switch in rice (*Oryza sativa*) (Wang et al., 2008; Zhang et al., 2012).

Both BZR1 and BES1 bind their target genes to activate BR responses (Yu et al., 2008; Li et al., 2009b; Luo et al., 2010; Sun et al., 2010). BES1 recruits two jumonji N/C (JmjN/C) domain-containing proteins, EARLY FLOWERING6 (ELF6) and RELATIVE OF EARLY FLOWERING6 (REF6), which are histone H3 Lys 27 demethylases (Yu et al., 2008; Lu et al., 2011). ELF6 and REF6 genetically influence flowering (Noh et al., 2004; Lu et al., 2011). However, much less is known about how BZR1 directly regulates flowering at the molecular level.

The cyclophilin (CYP) protein family includes cyclosporin A binding immunophilins as well as FK506 binding proteins (FKBPs) and parvulins (Lu and Armstrong, 2007). Immunophilins with peptidyl-prolyl *cis-trans* isomerase (PPIase) activity serve as protein folding catalysts by regulating *cis* and *trans* peptide-bond conformations of Pro residues in proteins (Matouschek et al., 1995). CYP family members are involved in hormone-mediated plant development. For example, the lack of *CYP40* causes defects in the transition from juvenile to adult stages of vegetative development and inflorescence morphological features in *Arabidopsis* (Berardini et al., 2001). In addition, CYP ROTAMASE CYCLOPHILIN1 (AtCYP18-3) is involved in BR signaling (Trupkin et al., 2012). Previously, we identified CYP20-2 as participating in GA signaling in wheat (*Triticum aestivum*). Accumulation of Ta CYP20-2 caused repressed GA-mediated DELLA protein degradation, suppressing cell elongation (Li et al., 2010a). DELLAs are mediators of signaling crosstalk between BRs and GAs in the regulation of cell elongation and plant growth (Li et al., 2012). DNA microarray assays of BR signaling revealed expression
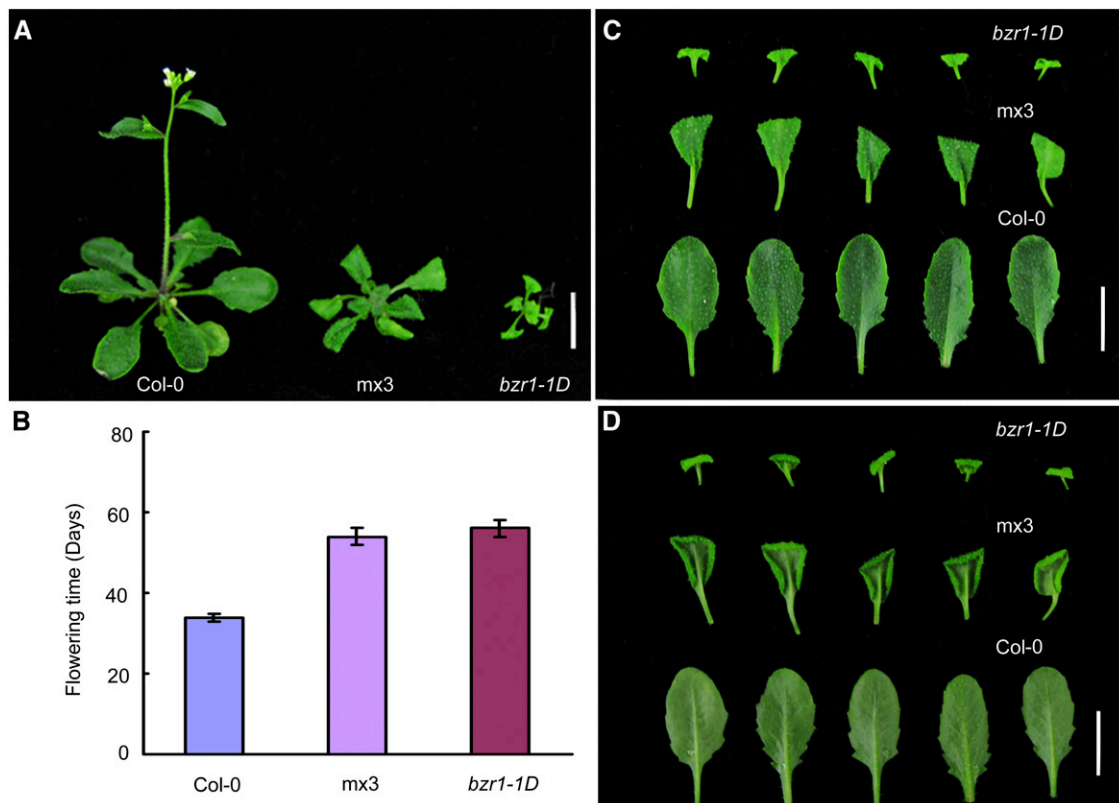
Figure 1. Late Flowering Phenotypes of mx3 and *bzr1-1D*.

(A) and **(B)** Phenotype **(A)** and flowering time **(B)** of mutants (mx3 and *bzr1-1D*) and the wild type (Col-0) grown under long-day (LD) conditions. Twenty plants were scored. Data are mean ± SD. Bar = 1 cm.
(C) and **(D)** Phenotypes of rosette leaves in the obverse **(C)** and reverse **(D)** view. Bar = 1 cm.

changes of a series of CYP family genes in *Arabidopsis*, such as *CYP20-2* and *FKBP13* (Sun et al., 2010). However, how CYPs function in BR signaling remains unclear.

Here, we report that BZR1 directly regulates *FLD* to mediate flowering. The conformation of BZR1 is altered by CYP20-2. Differences in activity and substrate preference of CYP20-2 from *Arabidopsis* and wheat led to altered flowering patterns. Thus, conformational changes of BZR1, mediated by CYP, may directly regulate the expression of *FLD* to influence flowering.

RESULTS

The *FLD* Gene Is a Direct Target of BZR1

We examined the transgenic *Arabidopsis* line *pBZR1:mBZR1-CFP* (for cyan fluorescent protein; mx3), which expresses a version of BZR1 in which Pro-234 is substituted with Leu-234 (Wang et al., 2002). The mx3 line showed a *bzr1-1D*-like phenotype, with reduced stature, slightly darker green and wider
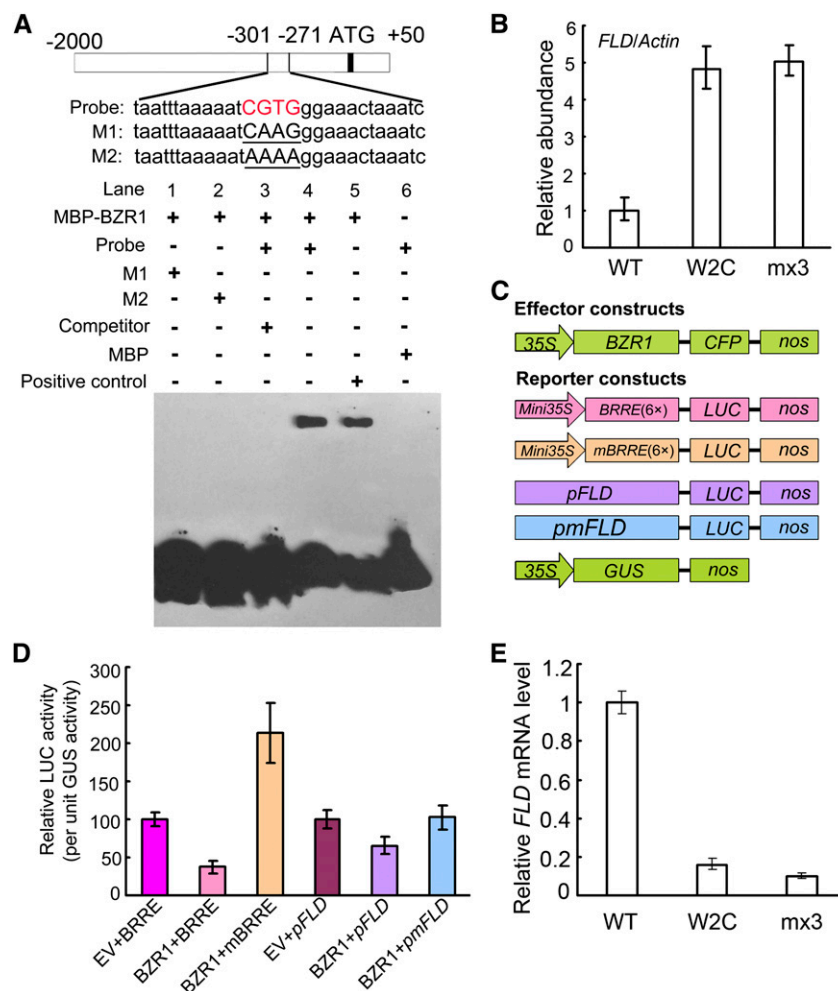
Figure 2. BZR1 Binds to the Promoter of *FLD*.

(A) EMSA assay in vitro showing that the MBP-BZR1 fusion protein, but not MBP alone, binds to the *FLD* promoter (Probe). The diagram depicts the promoter sequence of the *FLD* gene. The red letters represent the hypothetical binding element (CGTG). M1, CGTG was mutated as CAAG; M2, CGTG was mutated as AAAA. Competitor indicates 200-fold excess unlabeled competitor probe added to compete with the labeled probe. Positive control, probe designed according to the core binding *cis*-element of BZR1 with flank sequences deposited in the *CONSTITUTIVE PHOTOMORPHOGENIC DWARF* (*CPD*) promoter (CAGAAACCCCCCGTGTGCCC). The amount of MBP-BZR1 was 0.5 μg for lane 5 and 2 μg for the other lanes.
(B) ChIP assay with antibody to GFP. Quantitative real-time PCR analysis of products immunoprecipitated from wild-type (WT), BZR1-CFP (W2C), and mBZR1-CFP (mx3) transgenic plants. Data are mean ± SD of triplicate experiments.
(C) Schematic diagrams of reporter and effector constructs used in the protoplast transcription system.
(D) Expression activity assay of BRRE-, mBRRE-, *pFLD*-, and *pmFLD-LUC* reporter genes in *Arabidopsis* protoplasts transformed with the plasmid *35S:BZR1* or empty vector (EV), with *35S:GUS* as an internal control. Data are mean ± SD of triplicate experiments.
**(E)** *FLD* transcript levels in the wild-type, *pBZR1:BZR1-CFP* (W2C), and *pBZR1:mBZR1-CFP* (mx3) transgenic plants. Data are mean ± SD of triplicate experiments.

leaves, and shorter petioles and hypocotyls, as well as curly leaves and later flowering, compared with the wild type (Figures 1A to 1D). Both *bzr1-1D* and mx3 showed delayed flowering compared with the wild type under a long-day photoperiod (Figure 1B).

To obtain a global view of potential targets of BZR1 among flowering genes, the sequences 1 kb upstream of transcription start sites in flowering genes (Fornara et al., 2010) were examined for the presence of the key BR response *cis*-element (BRRE; CGTGNG) (He et al., 2005). In total, 17 of the 174 genes examined displayed sequences with high-confidence identity to BRRE in their promoters. These genes are involved in regulating several flowering pathways (see Supplemental Table 1 online). A putative BRRE, CGTGGG, was identified in the promoters of *FLD* at -287 to -281 and *FY* at -11 to -5, but not in any of the other known members of the autonomous pathway. However,

the expression of *FY* was not changed in the transgenic line *pBZR1:BZR1-CFP* (W2C) nor in mx3 compared with the wild type (see Supplemental Figure 1 online). Therefore, we focused on *FLD* as a candidate target of the transcription factor BZR1.

Electrophoretic mobility shift assay (EMSA) revealed that the putative BRRE from the *FLD* promoter (CGTGGG) was bound by MBP-BZR1, but not by maltose-binding protein (MBP) alone. The unlabeled putative BRRE probe competed away the binding to the labeled BZR1 protein (Figures 2A and 2B). Chromatin immunoprecipitation (ChIP) assays revealed that the promoter sequence of *FLD* was enriched by immunoprecipitation of CFP-tagged BZR1 (Figure 2C). Transcriptional activity assays in protoplasts revealed that expression of *BZR1* reduced the expression of *LUC* driven by either the native *FLD* promoter (including the putative BRRE CGTGGG) or repeated BRRE elements. By contrast, *LUC* expression driven by a mutated *FLD* promoter
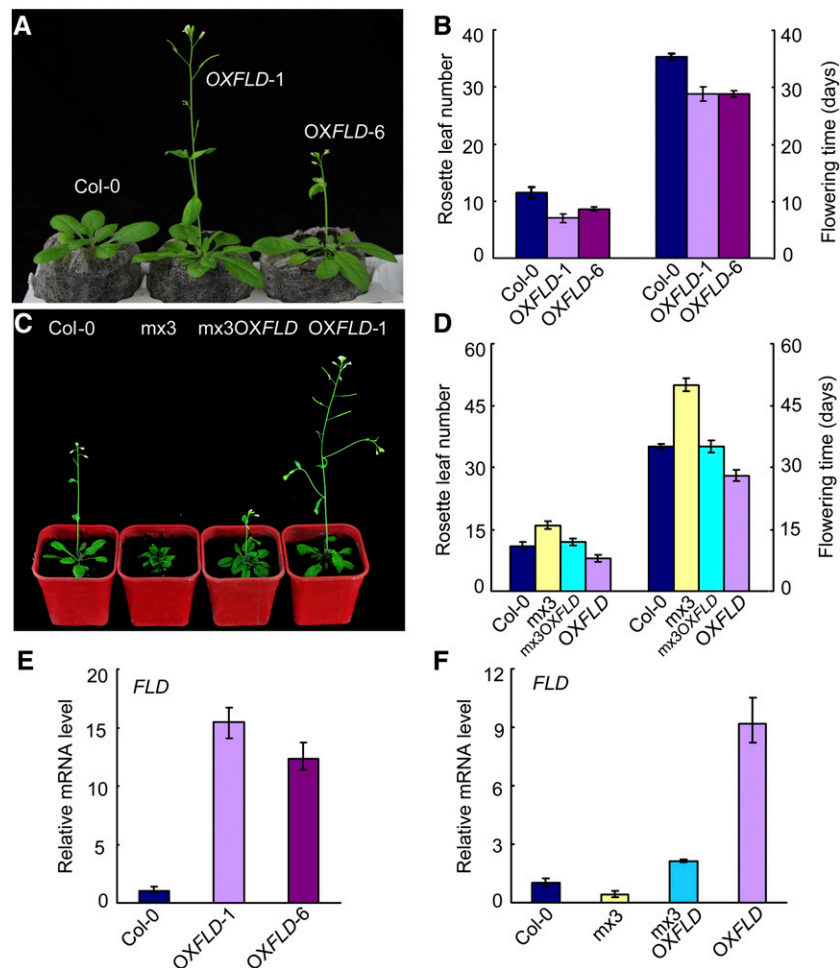
Figure 3. OX*FLD* Transgenic *Arabidopsis* Shows an Early Flowering Phenotype and Partially Rescued the Late Flowering Phenotype of mx3.

(A) and **(B)** Flowering phenotype of Col-0, OX*FLD*-1, and OX*FLD*-6 transgenic lines grown in light under long-day conditions for 27 d. Data are mean ± SD. For each line, 25 plants were scored.
(C) and **(D)** Flowering phenotype of Col-0, mx3, mx3 OX*FLD*, and OX*FLD Arabidopsis* grown in light under long-day conditions for 35 d. Data are mean ± SD. For each line, 20 plants were scored.
(E) and **(F)** Quantitative RT-PCR analysis of *FLD* transcript in transgenic lines and Col-0. Data are mean ± SD of triplicate experiments.

with A̲G̲A̲G̲A̲G̲ in place of the BRRE was not affected by *BZR1* expression. When driven by mBRRE, in which repeated copies of BRRE were each mutated to C̲A̲TGGG, *LUC* expression increased with *BZR1* expression (Figures 2D and 2E). In both *pBZR1: BZR1* (W2C) and *pBZR1:mBZR1^Pro234-Leu^-CFP* (mx3), *FLD* transcript accumulation was substantially decreased compared with the wild type (Figure 2F). Thus, BZR1 binds the putative BRRE in the promoter of *FLD* to suppress its transcriptional expression.

Either *35S:FLD* or *pmFLD:FLD* Can Partially Rescue the Late Flowering Phenotype of mx3

FLD was constitutively expressed under the control of a cauliflower mosaic virus (CaMV) 35S promoter in transgenic *Arabidopsis* lines

(OX*FLD*). The OX*FLD* lines showed an early flowering-time phenotype compared with the wild type under a long-day photoperiod (Figures 3A and 3B). When we crossed OX*FLD* with mx3, all F1 generation plants showed earlier flowering than mx3 but later flowering than OX*FLD* (Figures 3C and 3D). The transcript level of *FLD* in mx3 OX*FLD* was higher than that in mx3 but lower than that in OX*FLD* (Figures 3E and 3F). Therefore, the late flowering of mx3 was partially rescued by the overexpressed *FLD* in mx3 OX*FLD*. These data suggest that *BZR1* is functionally dependent on *FLD*.

To confirm further the genetic relationship between *BZR1* and *FLD*, *FLD* was expressed under control of either its native promoter (*pFLD:FLD*) or the mutated version (*pmFLD:FLD*) in various genetic backgrounds. Either *pFLD:FLD* or *pmFLD:FLD* could rescue the late flowering phenotype of *fld-4*, which is mutated in
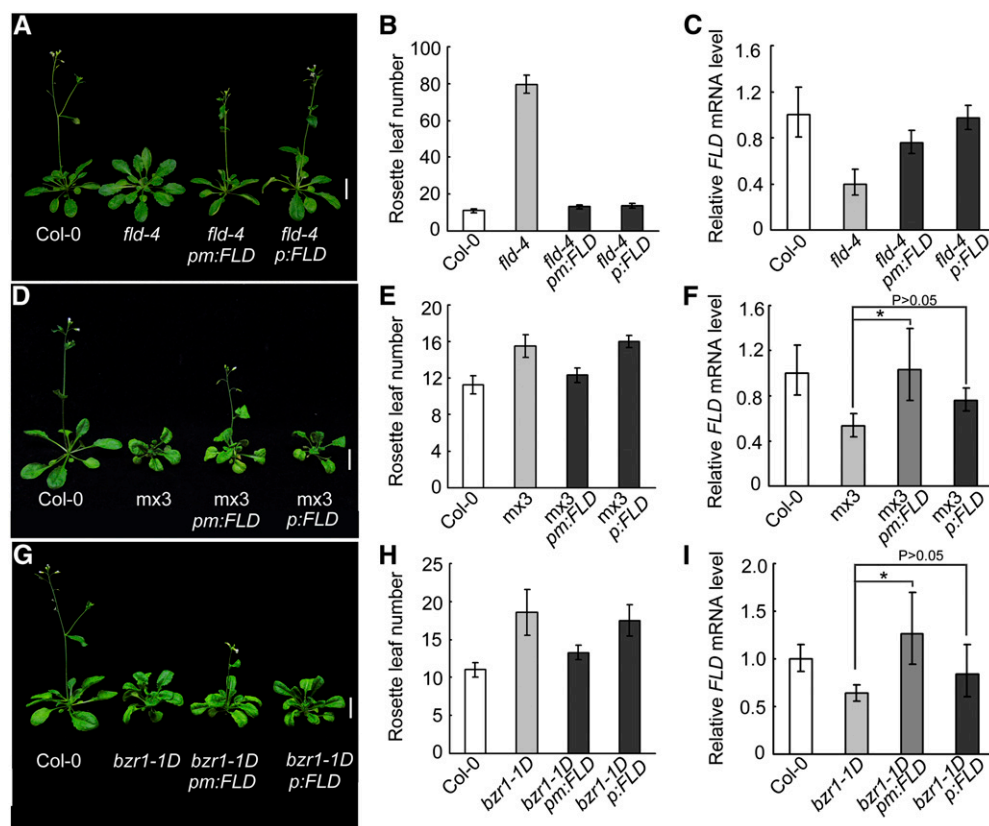
Figure 4. *pmFLD:FLD* Partially Rescued the Late Flowering Phenotype of mx3.

(A) and **(B)** Flowering phenotype of Col-0, *fld-4*, *fld-4 pm:FLD*, and *fld-4 p:FLD* transgenic lines grown in the light for 35 d under long-day conditions. Data are mean ± SD. For each line, 20 plants were scored. Bar = 1 cm.
(C) Quantitative RT-PCR analysis of *FLD* transcript in transgenic lines and the wild type.
(D) and **(E)** Flowering phenotype of Col-0, mx3, mx3 *pm:FLD*, and mx3 *p:FLD Arabidopsis* grown in the light under long-day conditions for 35 d. Data are mean ± SD. For each line, 20 plants were scored. Bar = 1 cm.
(F) Quantitative RT-PCR analysis of *FLD* transcript in transgenic lines and the wild type. Data are mean ± SD of triplicate experiments. *P < 0.05 and P > 0.05 compared with their parent mx3, respectively, as determined by Student's *t* test.
(G) and **(H)** Flowering phenotype of Col-0, *bzr1-1D*, *bzr1-1D pm:FLD*, and *bzr1-1D p:FLD Arabidopsis* grown in the light under long-day conditions for 35 d. Data are mean ± SD. For each line, 20 plants were scored. Bar = 1 cm.
(I) Quantitative RT-PCR analysis of *FLD* transcript in transgenic lines and Col-0. Data are mean ± SD of triplicate experiments. *P < 0.05 and P > 0.05 compared with their parent *bzr1-1D*, respectively, as determined by Student's *t* test.
pm:FLD, *pmFLD:FLD* (*FLD* expression driven by the native promoter of *FLD* with the BRRE mutated to AGAGAG); *p:FLD*, *pFLD:FLD* (*FLD* expression driven by the native promoter of *FLD* with a wild-type BRRE). Data are mean ± SD of triplicate experiments.

a flowering gene homologous to *LSD1* (Liu et al., 2007) (Figures 4A to 4C). The double transgenic line mx3 *pFLD:FLD* showed a similar flowering pattern to that of mx3 (Figures 4D to 4F). By contrast, the mx3 *pmFLD:FLD* line, with increased *FLD* transcript, showed earlier flowering compared with mx3. Similar results were obtained in the *bzr1-D* background. Whereas *bzr1-1D pFLD:FLD* showed no difference in flowering time compared with *bzr1-1D*, *bzr1-1D pmFLD:FLD* flowered earlier (Figures 4G to 4I). Therefore, the late flowering phenotypes of mx3 and *bzr1-1D* were rescued by *pmFLD:FLD*. Together, these data indicate that BZR1 contributes to *FLD* regulation to mediate flowering.
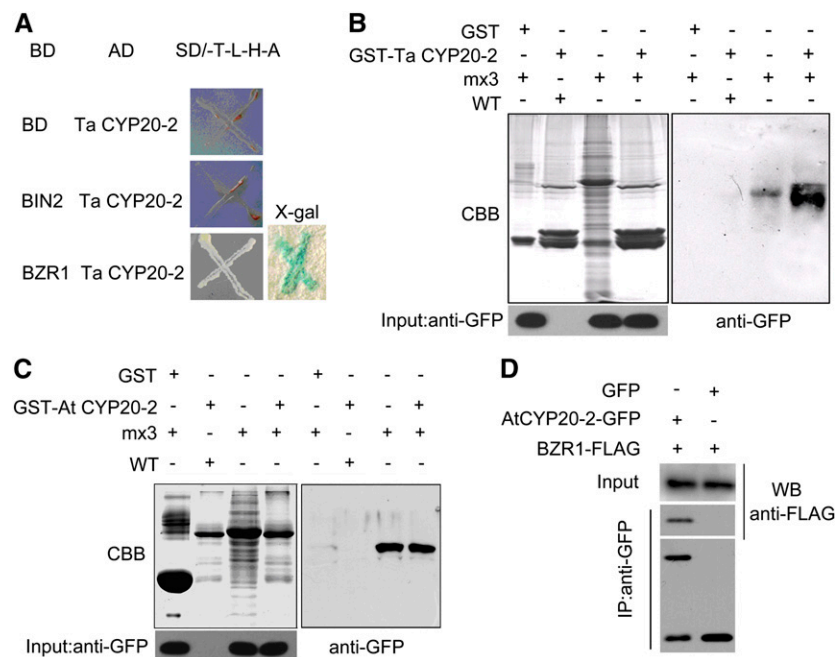
Interaction of CYP20-2 and BZR1

In our previous screen for proteins interacting with BZR1, a cyclophilin was identified as one of the potential targets. In yeast two-hybrid assays performed to confirm the interaction between BZR1 and CYP20-2, yeast cells cotransformed with pGBKT7-BZR1 and pGADT7-TaCYP20-2 were able grow on SD/-His-Trp-Leu-Ade selection medium and showed positive staining for β-galactosidase activity. Yeast cells harboring pGADT7-TaCYP20-2 along with pGBKT7-BIN2 or pGBKT7 failed to grow on the

same medium (Figure 5A). To confirm the interaction in vivo, the *pBZR1:mBZR1^Pro234-Leu-CFP* (mx3) transgenic line was used for pull-down assays. CFP-tagged mBZR1 bound to both gluta-thione *S*-transferase (GST)-TaCYP20-2 and GST-AtCYP20-2 but not GST alone under the same conditions (Figures 5B and 5C). Furthermore, when CYP20-2-YFP (for yellow fluorescent protein) and BZR1-FLAG fusion proteins were transiently coexpressed in tobacco (*Nicotiana tabacum*) leaf cells (Figure 5D), BZR1-FLAG could be coimmunoprecipitated with CYP20-2-YFP. Thus, CYP20-2 can interact with BZR1 in vivo.

Overexpression of *CYP20-2* Led to a Change in Flowering Time

At *CYP20-2* overexpression lines (AOX-2 and AOX-3) showed early flowering compared with the wild type either under a long-day or short-day photoperiod (Figures 6A to 6D). By contrast, neither the *cyp20-2* and *fkbp13* single mutants nor the double mutant *cyp20-2 fkbp13* differed from the wild type in flowering time (Figures 6A to 6E), which may be explained by the redundant function of other family members (Edvardsson et al., 2007). In the At *CYP20-2*–overexpressing lines, *FLC* expression

Figure 5. Protein Interaction between CYP20-2 and BZR1.

(A) Interaction between Ta CYP20-2 and At BZR1 in yeast two-hybrid assays. Colonies of yeast containing the indicated combination of bait (BD) and prey (AD) vectors were cultured on -Trp-Leu-His-Ade selection medium. β-Galactosidase activity of positive clones was analyzed by use of X-gal.
(B) Pull-down assay to confirm the interaction between Ta CYP20-2 and At BZR1. Glutathione agarose beads containing GST or GST-TaCYP20-2 were incubated with equal amounts of protein extract from mx3. Proteins bound to Sepharose 4B beads were pelleted, subjected to 12% SDS-PAGE, stained with Coomassie blue (CBB; left), and detected by immunoblot analysis with anti-GFP monoclonal antibody (right). WT, the wild type.
(C) Pull-down assay to confirm the interaction between At CYP20-2 and BZR1. Glutathione agarose beads containing GST or GST-AtCYP20-2 were incubated with equal amounts of protein extract from mx3. Proteins bound to Sepharose 4B beads were pelleted, subjected to 12% SDS-PAGE, stained with Coomassie blue (left), and detected by immunoblot analysis with anti-GFP monoclonal antibody (right).
(D) Coimmunoprecipitation assay to confirm the interaction between At CYP20-2 and BZR1. Tobacco leaves cotransformed with *35S:AtCYP20-2-YFP* and *35S:BZR1-FLAG* were used in immunoprecipitation assays with anti-GFP antibody, and the immunoblot was probed with anti-FLAG antibody.

was extremely downregulated, whereas *SOC1* expression was upregulated (Figure 6F). *FLD*, a negative regulator of *FLC*, was upregulated in AOX-2 and AOX-3 (Figure 6F). Thus, the expression of *FLD* to regulate flowering might be mediated by *CYP20-2*.

CYP40, a homolog of CYP20-2 (Li et al., 2010a), promotes the transition from juvenile to adult stages in *Arabidopsis* (Berardini et al., 2001). To test whether its activity was responsible for the lack of change in flowering time in the *cyp20-2 fkbp13* double mutant, *CYP40* was knocked down in the *cyp20-2 fkbp13* background using RNA interference. The *cyp20-2 fkbp13 cyp40RNAi* lines showed late flowering compared with their background *cyp20-2 fkbp13* (see Supplemental Figure 2 online). These results imply that members of the CYP gene family are required for, and redundantly act in, promotion of flowering.

Ectopic overexpression of Ta *CYP20-2* in *Arabidopsis* (TOX-6 and TOX-10) led to delayed flowering under long-day or short-day conditions (Figures 7A, 7B, and 7E). After vernalization treatment (4°C for 40 d), Ta*CYP20-2*–overexpressing lines and the wild type did not differ in flowering time (Figure 7C). It is worth noting

that GA$_3$ treatment rescued the delayed flowering of Ta *CYP20-2*–overexpressing transgenic plants (Figure 7D). These phenotypes were reminiscent of those of autonomous pathway mutants, such as *skb1* and *fca* (Mouradov et al., 2002; Lim et al., 2004; Wang et al., 2007). This result suggests that the GA pathway is involved in the control of flowering time, although BR signaling is involved in this process in the Ta *CYP20-2* transgenic lines.

To explore the molecular mechanism of late flowering, we examined the transcript levels of critical genes in flowering pathways. Expression of the flowering repressor *FLC* was upregulated in Ta *CYP20-2*–overexpressing plants (see Supplemental Figure 3 online). *SOC1*, which is inhibited in an *FLC*-dependent manner, was downregulated in the transgenic plants (see Supplemental Figure 3 online). This phenotype corresponded to the Ta CYP20-2 protein level of transgenic lines (Figures 7E and 7F). The *flc-3* Ta *CYP20-2* line showed a flowering pattern similar to that of the wild type (see Supplemental Figure 3 online). Thus, the function of Ta *CYP20-2* in flowering may depend on the *FLC*-mediated pathway in the transgenic lines. On the other hand, Ta CYP20-2 but not At CYP20-2 interacted with a DELLA (RGA, REPRESSOR OF GA1-3)
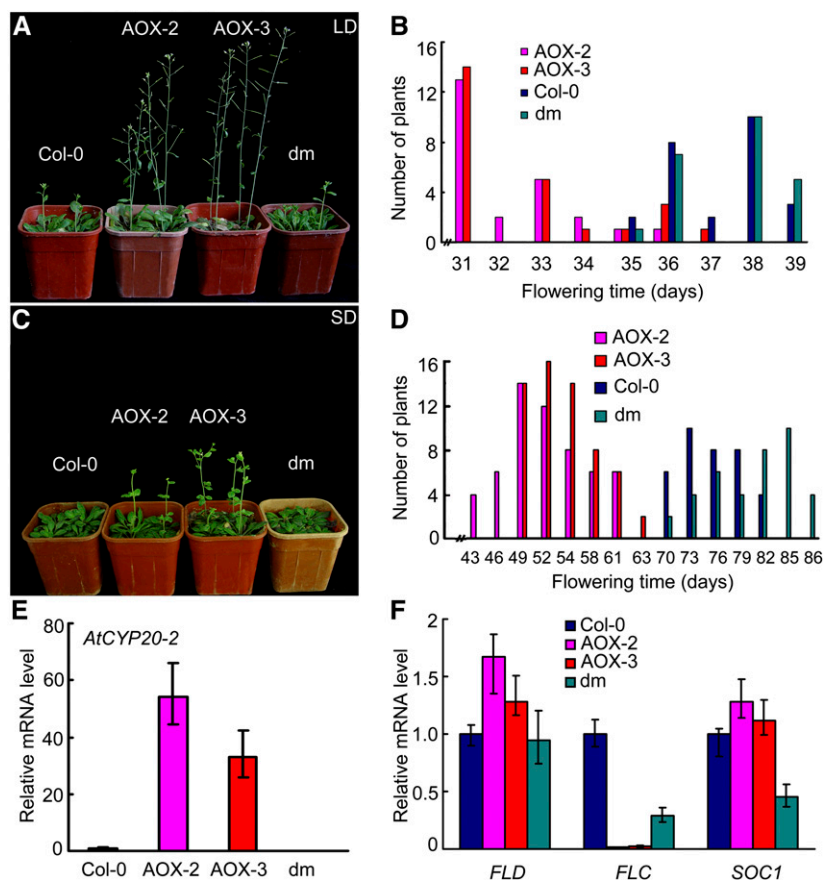
Figure 6. Flowering Phenotypes of *35S*:At*CYP20-2* Transgenic *Arabidopsis*.

(A) to **(D)** The phenotype and time of flowering of Col-0, *35S*:At*CYP20-2* (AOX-2 and AOX-3), and *cyp20-2 fkbp13* (dm) *Arabidopsis* grown under long-day conditions (**[A]** and **[B]**) or short-day conditions (**[C]** and **[D]**). Twenty-five plants were scored.
(E) and **(F)** Quantitative RT-PCR analysis of At *CYP20-2*, *FLD*, *FLC*, and *SOC1* in Col-0, *35S*:At*CYP20-2* overexpression lines, and *cyp20-2 fkbp13* (dm). Data are mean ± SD (*n* = 3).
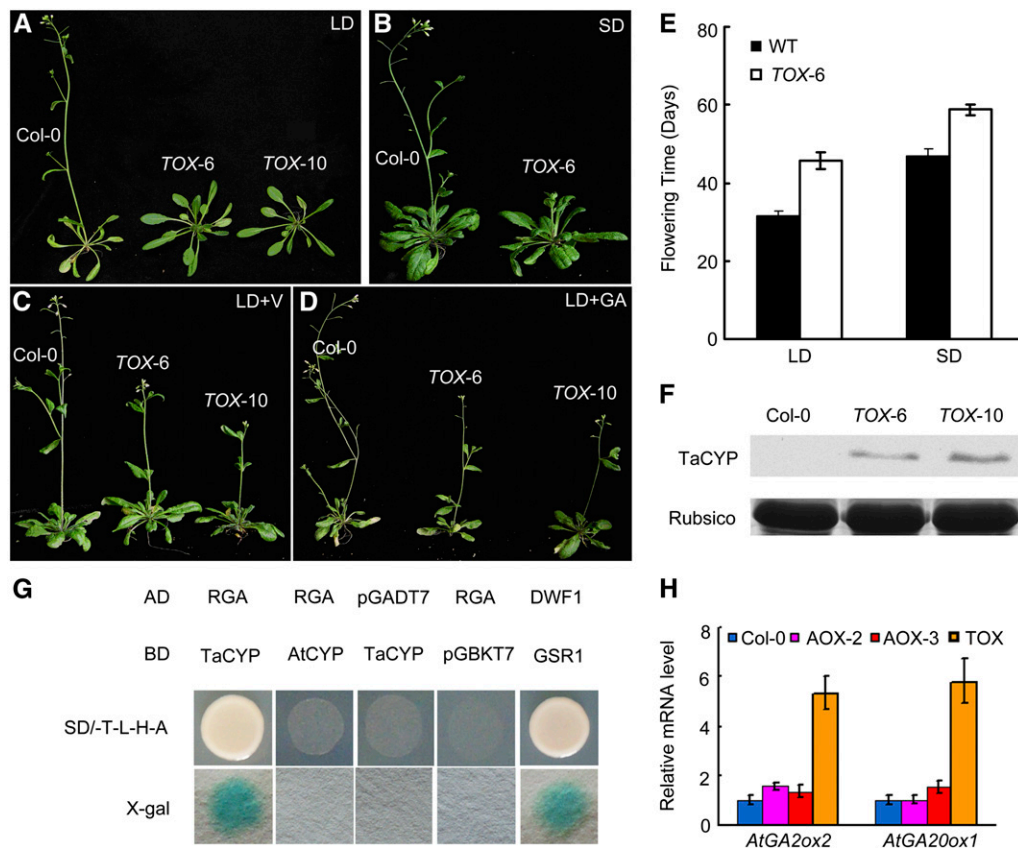
Figure 7. Flowering Phenotype of *35S*:Ta*CYP20-2* Transgenic *Arabidopsis*.

(A), **(B)**, and **(E)** The flowering phenotypes in wild-type (WT; Col-0) and *35S*:Ta*CYP20-2* (TOX-6 and TOX-10) transgenic *Arabidopsis* grown under long-day (LD) **(A)** or short-day (SD) conditions **(B)** for 40 d after germination. Twenty plants were scored. Data are mean ± SD.

(C) and **(D)** Effect on flowering of vernalization (V) **(C)** or GA treatment **(D)**.

(C) Col-0 and *35S*:Ta*CYP20-2* transgenic *Arabidopsis* grown at 4°C for 4 weeks and moved to LD conditions for 30 d.

(D) Plants were treated with GA$_3$ (20 μM) and grown under long-day conditions.

(F) Immunoblot analysis of Ta CYP20-2 protein expression in Col-0 and *35S*:Ta*CYP20-2*–overexpressing transgenic *Arabidopsis* with polyclonal anti-TaCYP20-2 antiserum. Total protein stained with Coomassie blue (ribulose-1,5-bisphosphate carboxylase/oxygenase [Rubisco]) shows equal loading.

(G) Protein interaction between Ta CYP20-2/At CYP20-2 and the DELLA protein RGA was tested by yeast two-hybrid assays. The clones of yeast containing each combination of bait (BD) and prey (AD) vectors were cultured on -Trp-Leu-His-Ade selection medium. β-Galactosidase activity of positive clones was analyzed by use of X-gal.

(H) Real-time RT-PCR analysis of the expression of GA biosynthesis genes At *GA2ox2* and At *GA20ox1* in *35S*:At*CYP20-2* and *35S*:Ta*CYP20-2* transgenic lines. The mean ± SD of three experiments is shown.

in yeast two-hybrid assays (Figure 7G). In addition, the expression levels of GA pathway genes *GA20ox1* and *GA2ox2* were increased in the later-flowering Ta *CYP20-2* overexpression lines (Figure 7H). This is consistent with hypothesis that both GA and BR signaling contribute to later flowering in the Ta *CYP20-2* overexpression *Arabidopsis* lines.

CYP20-2 Enhances Phosphorylation of BZR1

To determine whether there were differences in activity between Ta CYP20-2 and At CYP20-2, we tested BR signaling in various plant lines. We crossed Ta *CYP20-2* overexpression lines or At *CYP20-2* overexpression lines with mx3 *Arabidopsis*. Except for mx3, all lines showed hypocotyl lengths similar to that of the

wild type in the dark (Figure 8A). Upon treatment with the BR biosynthesis inhibitor brassinazole (Brz) (0.5 μM) in the dark, the mx3 *35S*:Ta*CYP20-2* (mx3 Ta) line showed closed cotyledons similar to mx3; however, cotyledons were open in mx3 *35S*:At-*CYP20-2* (mx3 At) under the same conditions, which was similar to the wild type (Figure 8B). When the concentration of Brz was increased to 2 μM, both mx3 Ta and mx3 At showed the same response as the wild type (Figures 8C to 8E). Compared with the wild type, mx3 Ta plants showed coiled leaves. However, the phenotype was weaker and plants flowered earlier than mx3 plants (Figures 8F, 8G, and 8I). In mx3 At, the coiled leaf phenotype was partially rescued (Figures 8H to 8J). Thus, the phenotypes caused by overexpression of mBZR1 were genetically impaired by overexpression of *CYP20-2*. However, At

CYP20-2 made a larger contribution to the BR-signaling phenotype than did Ta *CYP20-2* in the transgenic lines.

At the transcriptional level, *BZR1* expression was greater in mx3 and in the crossed plants than in the wild type (Figure 9A). The relative amount of BZR1 protein was higher in mx3 and mx3 Ta than in the wild type but lower in mx3 Ta and mx3 At than in mx3 plants (Figures 9B and 9C). mx3 was treated with BL, and the amount of unphosphorylated and phosphorylated mBZR1 was monitored by immunoblotting. The result showed that there was more unphosphorylated mBZR1 upon BL treatment, with the intensity of the bands similar to those in Figure 9C (see Supplemental Figure 4 online). The ratio of phosphorylated to unphosphorylated mBZR1 was 0.58, 0.60, and 1.68 in mx3 Ta, mx3, and mx3 At lines, respectively (Figure 9E). Transcriptional activity assays in protoplasts revealed that constitutive expression of either Ta *CYP20-2* or At *CYP20-2* impaired the function

of BZR1 (Figure 9D). Therefore, CYP20-2 may accelerate phosphorylation on mBZR1 for degradation by the ubiquitin-proteasome system, and At CYP20-2 may be more effective in this process than Ta CYP20-2.

The Secondary Structure Composition of BZR1 Changed upon Interacting with CYP20-2

A time course of PPIase enzyme activity of the recombinant proteins GST-TaCYP20-2 (52 kD) and GST-AtCYP20-2 (52 kD) (Figure 10A) clearly showed that GST-AtCYP20-2 had greater PPIase activity than did GST-TaCYP20-2 (Figure 10B). Fourier transform infrared (FTIR) spectroscopy was used to monitor any changes in the secondary structure composition of BZR1 in the presence of GST-TaCYP20-2 or GST-AtCYP20-2. In the secondary derivative spectra, BZR1 showed a number of typical absorption peaks
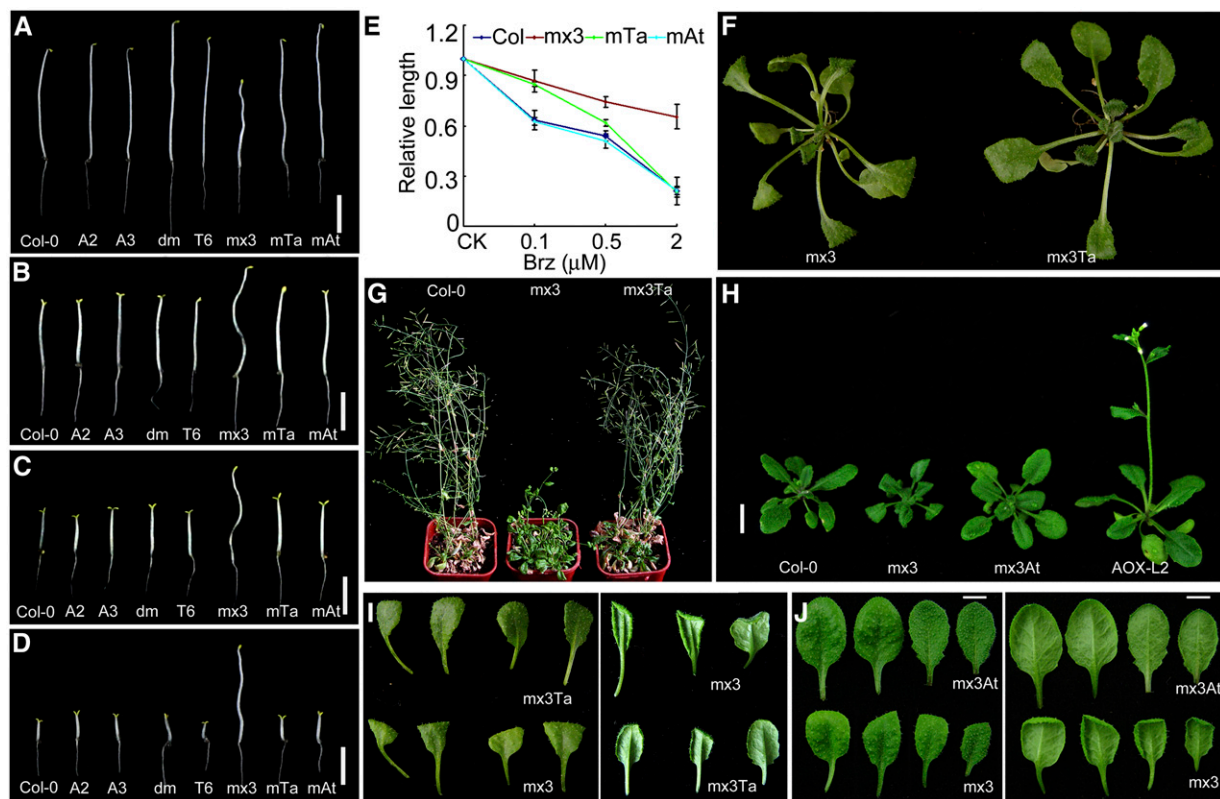
Figure 8. *35S*:*CYP20-2* Partially Rescued the BR-Related Phenotype in mx3.

(A) Six-day-old dark-grown seedlings. From left to right: Col-0, A2 (*35S*:At*CYP20-2* L2), A3 (*35S*:At*CYP20-2* L3), dm (*cyp20-2 fkbp13*), T6 (*35S*: Ta*CYP20-2* L6), mx3 (*pBZR1*:m*BZR1-CFP*), mx3Ta:mx3 *35S*:Ta*CYP20-2*, and mx3At:mx3 *35S*:At*CYP20-2*. Bar = 1 cm.
(B) to **(D)** Seedlings were grown in the dark for 6 d with various concentrations of Brz, 0.1 μM **(B)**, 0.5 μM **(C)**, and 2 μM **(D)**. From left to right: Col-0, A2 (*35S*:At*CYP20-2* L2), A3 (*35S*:At*CYP20-2* L3), dm (*cyp20-2 fkbp13*), T6 (*35S*:Ta*CYP20-2* L6), mx3 (*pBZR1*:m*BZR1-CFP*), mx3Ta:mx3 *35S*:Ta*CYP20-2*, and mx3At:mx3 *35S*:At*CYP20-2*. Bar = 1 cm.
**(E)** Relative length of hypocotyls. Twenty plants were measured. Data are mean ± sd.
(F) From left to right: mx3 and mx3 *35S*:Ta*CYP20-2* grown in the light for 25 d under long-day conditions.
(G) Col-0, mx3, and mx3 *35S*:Ta*CYP20-2* grown in the light for 50 d under long-day conditions.
(H) Col-0, mx3, *35S*:At*CYP20-2*, and mx3 *35S*:At*CYP20-2* grown in the light for 25 d under long-day conditions. Bar = 1 cm.
(I) Rosette leaves of mx3 and mx3 *35S*:Ta*CYP20-2* plants.
(J) From top to bottom line: Rosette leaves of mx3 *35S*:At *CYP20-2* and mx3 plants. mx3Ta, mx3 *35S*:Ta *CYP20-2*; mx3At, mx3 *35S*:At *CYP20-2*.
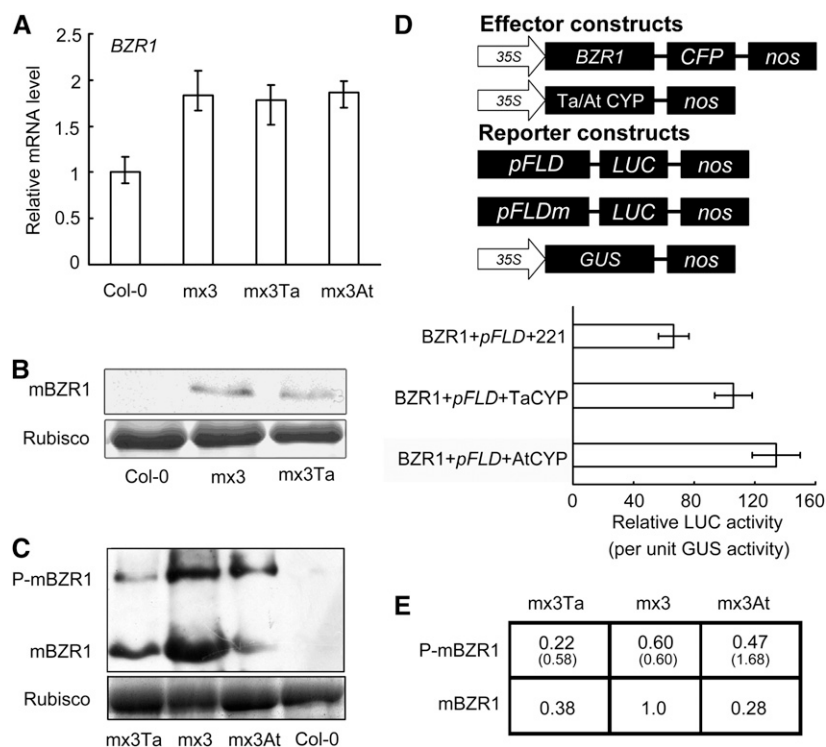
Figure 9. Effects of *CYP20-2* Expression on mx3 *Arabidopsis*.

(A) Real-time PCR of *BZR1* transcript in Col-0, mx3, mx3 *35S*:Ta*CYP20-2*, and mx3 *35S*:At*CYP20-2*. Data are mean ± SD (*n* = 3).

(B) Immunoblot analysis of mBZR1-CFP in Col-0, mx3, and mx3 *35S*:Ta*CYP20-2*. Total protein extracts were separated by 12% SDS-PAGE, and mBZR1-CFP was detected with anti-GFP polyclonal antibody. mx3 Ta, mx3 *35S*:Ta*CYP20-2*. Ribulose-1,5-bisphosphate carboxylase/oxygenase (Rubisco) served as a loading control in **(B)** and **(C)**.

(C) Immunoblot analysis of phosphorylation of mBZR1-CFP in Col-0, mx3, mx3 *35S*:Ta*CYP20-2*, and mx3 *35S*:At*CYP20-2*. In order to separate the p-mBZR1 and mBZR1, protein extracts were separated by 10% SDS-PAGE until proteins smaller than 55 kD were running off the gel. The proteins were detected with anti-GFP monoclonal antibody. mx3 Ta, mx3 *35S*:Ta*CYP20-2*; mx3At, mx3 *35S*:At*CYP20-2*.

(D) Expression activity assay of the *pFLD* reporter gene in *Arabidopsis* protoplasts transformed with the plasmid *35:BZR1* in the presence of *35S*:At*CYP20-2* or *35S*:Ta*CYP20-2*, with *35S*:*GUS* as an internal control. Data are mean ± SD of triplicate experiments.

(E) Both phosphorylated and unphosphorylated forms of BZR1 shown in **(C)** were quantified. In the table, the numbers represent the relative protein amounts using unphosphorylated forms of BZR1 in mx3 as 1.0. Numbers in parentheses represent the ratio of phosphorylated to unphosphorylated forms of BZR1.

(Figure 10C), which could be assigned to different types of secondary structure (Li et al., 2009a): 1625 cm^{-1} (β-sheet [β-sheet 1]), 1635 cm^{-1} (β-sheet [β-sheet 2]), 1642 cm^{-1} (random coil/loop [random coil/loop 1]), 1646 cm^{-1} (random coil/loop [random coil/loop 2]), and 1654 cm^{-1} (α-helices). Upon interaction with Ta CYP20-2, the secondary derivative peaks were 1623 cm^{-1} (β-sheet 1), 1628 cm^{-1} (β-sheet 2), 1644 cm^{-1} (random coil/loop 2), and 1653 cm^{-1} (α-helices). The assignments of the observed bands in both FTIR and time-resolved infrared spectra are summarized in Table 1. All absorption peaks of secondary structures for BZR1, except random coil 1 at 1642 cm^{-1}, were red shifted after binding with Ta CYP20-2; random coil 1 was blue shifted by 2 cm^{-1}. If we assume that the structure of Ta CYP20-2 is rigid, the secondary structure change would mainly come from BZR1.

The finding that most of BZR1 has a red shift in its absorption spectrum indicates that the secondary structure of BZR1 is opened to polar D$_2$O, the chemical formula of heavy water,

solvent. The presence of a blue-shifted peak (from 1642 to 1644 cm^{-1}) strongly suggests that the Ta CYP20-2 enzyme binds the substrate (BZR1) at this secondary structure (i.e., random coil/ loop 1). The blue shift is likely due to hydrophobic interaction between BZR1 and Ta CYP20-2. We suspected that Pro-234 in BZR1 was the core binding site of Ta CYP20-2 and in random coil/loop 1. To test this prediction, we used mBZR1 with Pro-234 substituted with Leu-234. Interestingly, the secondary derivative spectra of mBZR1 alone did not differ from that in the presence of Ta CYP20-2 (Figure 10D). Thus, Ta CYP20-2 may fail to bind mBZR1 as a substrate, which is consistent with our prediction that a mutation at this random coil/loop structure would destroy the binding site.

In contrast with the results with Ta CYP20-2, the presence of At CYP20-2 induced blue shifts in nearly all of the absorption peaks of BZR1, which implies that At CYP20-2 can bind BZR1 and induce opening in the secondary structure of BZR1. However, the structure of BZR1 became even tighter after binding to
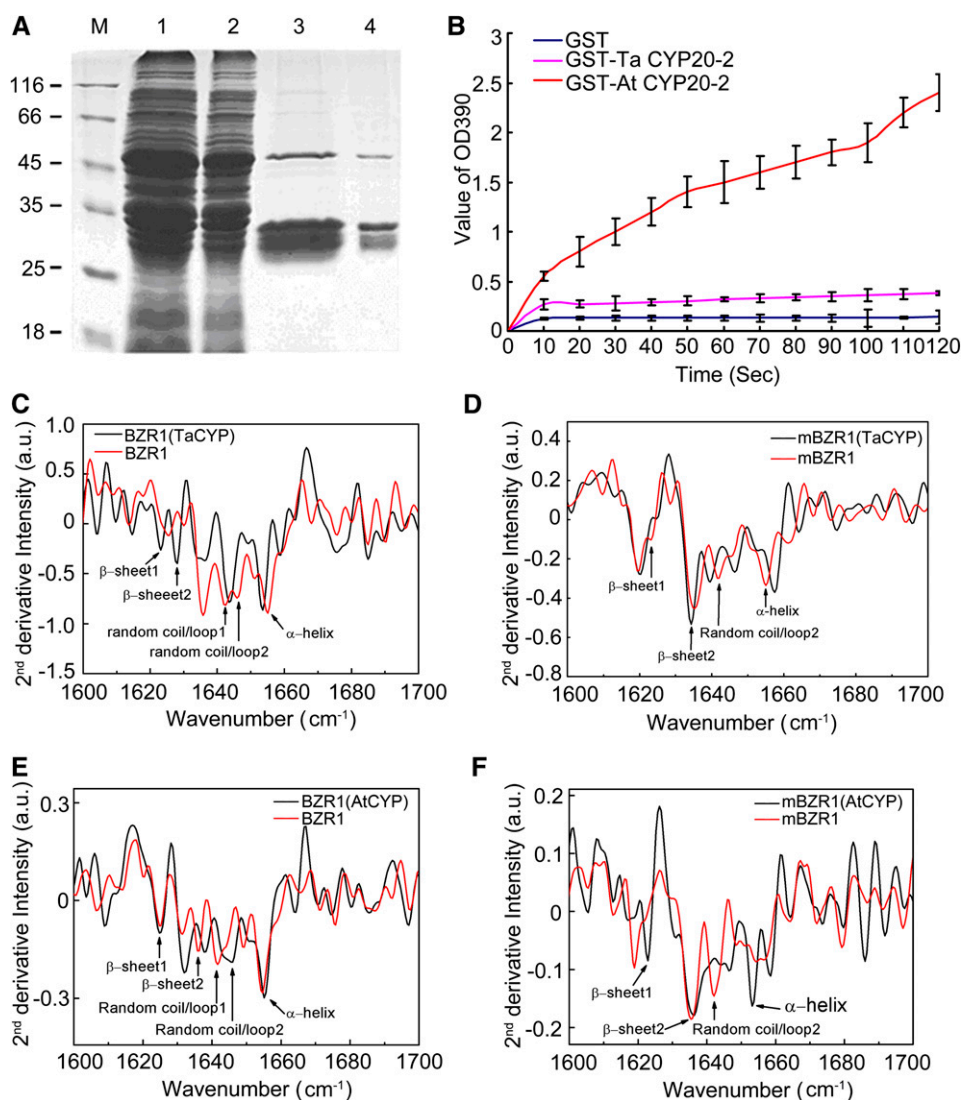
Figure 10. PPIase Activity of Ta CYP20-2 and At CYP20-2 and Their Effects on BZR1 Secondary Structure.

(A) Expression and purification of GST-TaCYP20-2 and GST-AtCYP20-2 recombinant protein. Lane 1, total protein of *DH5α* cells containing the pGEX4T-1-TaCYP20-2 plasmid. Lane 2, total protein of *DH5α* cells containing the pGEX4T-1-AtCYP20-2 plasmid. Lane 3, GST-TaCYP20-2 fusion protein purified by glutathione-Sepharose 4B chromatography. Lane 4, GST-AtCYP20-2 fusion protein purified by glutathione-Sepharose 4B chromatography.

(B) PPIase activity of recombinant Ta CYP20-2 (pink), At CYP20-2 (red), and GST (blue) at 10 nM. Data are mean $\pm$ SD (n = 3).

(C) Second-derivative infrared spectra of BZR1 with or without GST-TaCYP20-2. Shown are MBP-BZR1 + GST-TaCYP20-2 minus the background absorption of MBP + GST-TaCYP20-2 (black) and MBP-BZR1 + GST minus the background absorption of MBP + GST (red); spectra were obtained in D_2O medium. a.u., absorbance units.

(D) Second-derivative infrared spectra of mBZR1 with or without GST-TaCYP20-2. Shown are MBP-mBZR1 + GST-TaCYP20-2 minus the background absorption of MBP + GST-Ta CYP20-2 (black) and MBP-mBZR1 + GST minus the background absorption of MBP + GST (red); spectra were obtained in a D_2O medium.

(E) Second-derivative infrared spectra of BZR1 with or without GST-At CYP20-2. Shown are with MBP-BZR1 + GST-AtCYP20-2 minus the background absorption of MBP+GST-AtCYP20-2 (black) and MBP-BZR1 + GST minus the background absorption of MBP + GST (red); spectra were obtained in D_2O medium.

(F) Second-derivative infrared spectra of mBZR1 with or without GST-AtCYP20-2. Shown are MBP-mBZR1 + GST-AtCYP20-2 minus the background absorption of MBP + GST-AtCYP20-2 (black) and MBP-mBZR1 + GST minus the background absorption of MBP + GST (red); spectra were obtained in a D_2O medium.

Table 1. Assignment of the Observed Amide I' Band to Its Corresponding Secondary Structures

Observed (cm^{-1})			
BZR1	BZR1+CYP20-2	Assignment	Literature Values
1625	1623	β-Sheet 1	1630/1623 ~1641
1635	1628	β-Sheet 2	
1642	1640	Random coil/loop 1	1645/1640 ~1650
1646	1644	Random coil/loop 2	
1654	1653	α-Helices	1652/1650 ~1656

At CYP20-2 (Figure 10E). In addition, At CYP20-2 induced changes in the secondary derivative spectra of the mutant mBZR1 (Figure 10F). Therefore, there might be a binding site for At CYP20-2 in BZR1 different from that for Ta CYP20-2.

These results suggest that both Ta CYP20-2 and At CYP20-2 can alter the secondary structure conformation of BZR1. However, At CYP20-2 has a stronger and more specific effect than does Ta CYP20-2 in the conformational changes of the targets, which corresponds with its higher PPIase activity in vivo. A model for the function of CYP20-2 in altering the secondary structure of BZR1 is shown in Supplemental Figure 5 online.

Histone Modification on *FLC* Chromatin Changes Along With *FLD* Expression

The expression of *FLD* was higher in At *CYP20-2* overexpression lines than in the wild type, but there was less H3K4me3 and H3 acetylation (Figure 11A). By contrast, *FLD* was downregulated in 35S:Ta*CYP20-2* lines, and there was more H3K4me3 and H3 acetylation than in the wild type. In *pBZR1:BZR1-CFP* (W2C) and *pBZR1:mBZR1*$^{Pro234-Leu}$*-CFP* (mx3), *FLD* transcript was reduced and H3K4me3 and H3 acetylation were dramatically increased. By contrast, H3K4me3 and H3 acetylation was lower in the crossed progeny line mx3 Ta than in mx3 alone (Figure 11A). These data hint that the levels of H3K4me3 and H3 acetylation are negatively correlated with the expression of *FLD*, a putative demethylase gene, which is targeted by BZR1 via CYP20-2.

Compared with the wild type, *FLC* transcription was decreased in the earlier flowering AOX lines, but increased in the later flowering genetic lines, such as mx3 and TOX (Figures 11A and 11B). To examine the relationship between this and the levels of the activating marks H3K4me3 and H3 acetylation, we performed ChIP assays using the *fld-4* mutant as a positive control (Figure 11C). Consistent with the *FLC* expression levels, the 35S:At*CYP20-2* lines showed less H3K4me3 in nearly all regions of *FLC* chromatin and less H3 acetylation in region I of *FLC* chromatin compared with the wild type. Conversely, mx3 showed a higher level of chromatin modification than did the wild type, but a similar level to that of 35S:Ta*CYP20-2* lines. There was more modification in mx3 Ta than in mx3 At lines but less than in mx3 (Figure 11C). Therefore, both H3K4me3 and H3 acetylation in *FLC* chromatin were changed along with the transcript level of *FLD*. CYP20-2 modulated the conformation of BZR1, which targeted the promoter of *FLD* to regulate flowering in *Arabidopsis* (Figure 11D).

DISCUSSION

BZR1 Directly Represses *FLD* to Regulate Flowering in *Arabidopsis*

Our results show that core BRREs (CGTGT/CG) are bound by BZR1, which represses the transcription of *FLD* in *bzr1-1D* and mx3 *Arabidopsis*. *bzr1-1D* and mx3 transgenic *Arabidopsis* showed extremely late flowering. BZR1 may directly repress *FLD* expression to modulate *FLC* and regulate flowering. However, it is worth noting that the late flowering phenotype seen in *bzr1-1D* may have nothing to do with BR signal transduction from BRI1 and BAK1. The mutants of BR positive regulators, such as *bri1* and *bak1*, display late flowering phenotypes only when the expression levels of those regulators are decreased. Neither the expression level of *FLD* nor that of *BZR1* was altered in *bri1-5* (see Supplemental Figure 6 online) (Sun et al., 2010), even though it shows a late flowering phenotype. Therefore, the late flowering phenotype of *bzr1-1D* is not likely caused by BR signaling from BRI1 and BAK1. Although BES1 and BZR1 are important components in BR signaling, these two transcription factors are also regulated by other signaling molecules, such as GAs (Wang et al., 2002; Yin et al., 2002, 2005; He et al., 2005; Bai et al., 2012). Therefore, the molecular mechanism of flowering regulation by BZR1 is distinct from that of BRI1.

Since the expression of *FLD* was decreased in mx3 and *pBZR1:BZR1*, late flowering was expected in both mx3 and *pBZR1:BZR1*. However, *pBZR1:BZR1* did not cause obvious phenotypes on flowering time in the wild-type background (Wang et al., 2002) (see Supplemental Figure 7 online), but *pBZR1:mBZR1-CFP* (mx3) showed late flowering (Figure 1). Similarly, *pBZR1:BZR1* showed the same response to Brz in a hypocotyl elongation assay compared with the wild type, but the expression of *CPD* was decreased in *pBZR1:BZR1* (Gampala et al., 2007). All of these results may be due to the sustained BZR1 accumulation conferred by the *bzr1-1D* mutation in mx3 that is absent in *pBZR1:BZR1*.

Arabidopsis overexpressing At CYP20-2 showed early flowering with decreased *FLC* transcript and increased *FLD* (Figure 6). Loss of function of *FLD* increases the levels of di- and trimethylated H3K4 and core histone tail acetylation in *FLC* chromatin (He et al., 2003; Jiang et al., 2007; Liu et al., 2007). Di- and trimethylated H3K4 are associated with activation of *FLC* (He et al., 2004). The increased *FLD* expression in At *CYP20-2*–overexpressing lines was consistent with the
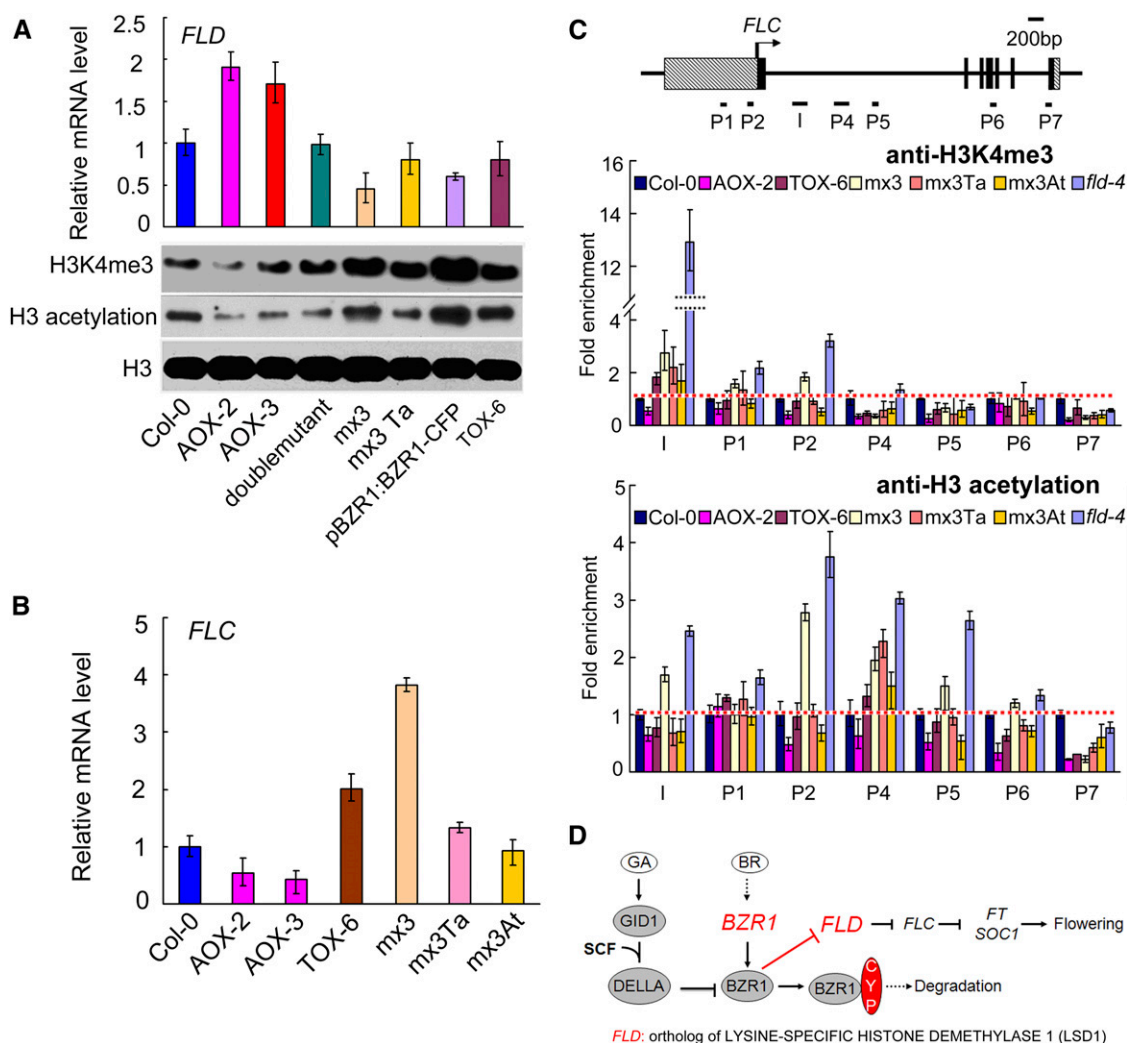
Figure 11. H3K4me3 and H3 Acetylation in *FLC* Chromatin Is Negatively Correlated with the Transcript Level of *FLD*.

(A) Quantitative RT-PCR of *FLD* in Col-0, AOX-2, AOX-3 (*35S*:At*CYP20-2*), double mutant (*cyp20-2 fkbp13*), mx3 (*pBZR1:mBZR1-CFP*), mx3Ta (mx3 *35S*:Ta*CYP20-2*), W2C (*pBZR1:BZR1-CFP*), and TOX-6 (*35S*:Ta*CYP20-2*) plants. Data are mean ± SD (*n* = 3). Immunoblot analysis of histone modification levels. Histone-enriched protein extracts from 2-week-old Col-0, AOX-2, AOX-3, mx3, mx3 *35S*:Ta*CYP20-2*, W2C, and TOX-6 plants grown under long-day conditions were probed with antibodies to H3K4me3 and H3 acetylation.

(B) Quantitative RT-PCR of *FLC* in Col-0, AOX-2, AOX-3 (*35S*:At*CYP20-2*), TOX-6 (*35S*:Ta*CYP20-2*), mx3 (*pBZR1:mBZR1-CFP*), mx3 Ta (mx3 *35S*: Ta*CYP20-2*), and mx3At (mx3 *35S*:At*CYP20-2*) plants. The mean ± SD of three experiments is shown.

(C) ChIP assay of the relative levels of trimethylated H3K4 (H3K4me3) and H3 acetylation in *FLC* chromatin. DNA fragments obtained by ChIP were analyzed by real-time PCR. The primer pairs used in PCR are shown as bars below the *FLC* gene structure; exons are shown as black boxes, introns as black lines, and untranslated regions as dashed boxes. Data are mean ± SD of triplicate experiments.

(D) Hypothetical model of CYP20-2 and BZR1 function in BR signaling and flowering pathways.

reduced level of trimethylated H3K4 and H3 acetylation in *FLC* chromatin (Figure 11). *FLD* is transcriptionally suppressed by BZR1. Consistent with this, trimethylated H3K4 and H3 acetylation were greatly increased in *pBZR1:mBZR1^Pro234-Leu_-CFP* and *pBZR1:BZR1-CFP* transgenic plants but returned to a normal level in mx3Ta *Arabidopsis* (Figure 11). On the other hand, FLD interacts with FCA and FPA for RNA 3′ processing to regulate flowering (Sonmez et al., 2011). Therefore, *FLC* may be one of the targets of FLD to regulate

flowering. *CYP20-2* therefore represents a component in the autonomous pathway of flowering.

CYP20-2 Alters the Conformation of BZR1 to Regulate Flowering

BZR1 may be involved in flowering via posttranscriptional regulation. The *BZR1* transcript level did not differ between mx3 *35S:CYP20-2* and mx3 alone (Figure 9), whereas the mBZR1

protein level in the crossed lines was markedly lower than in mx3. Furthermore, the expression of *CYP20-2* caused accumulation of the phosphorylated form of mBZR1, which could be degraded by the proteasome machinery in mx3 *35S:CYP20-2*. The CYP-like domain is specifically associated with subunit S1 of the 19S regulatory particle in the 26S proteasome to selectively promote the accumulation of properly folded targets of the ubiquitin-proteasome system for degradation (Yi et al., 2007). Our data suggest that CYP20-2 interacts with BZR1 (Figure 5) and alters its secondary structure to affect its phosphorylation status (Figures 9 and 10). Therefore, CYP20-2 may catalyze *cis-trans* isomerization of the peptide bond N-terminal to Pro residues in BZR1 to promote phosphorylation of BZR1, which can be degraded by a ubiquitin-proteasome system.

Since the PPIase activity of Ta CYP20-2 was weaker than that of At CYP20-2 (Figure 10B), Ta *CYP20-2* overexpression lines with increased *FLC* transcript showed late flowering (Figure 7; see Supplemental Figure 3 online). *FLD* transcript was slightly decreased in Ta *CYP20-2*–overexpressing lines, but trimethylated H3K4 and H3 acetylation in *FLC* chromatin was increased (Figure 11). The level of trimethylated H3K4 and H3 acetylation was lower in mx3 *35S:TaCYP20-2* than in mx3 (Figure 11). However, mx3 *35S:TaCYP20-2* was more insensitive to Brz than was mx3 *35S:AtCYP20-2*, which is more like mx3 (Figure 8). The alteration of signaling was weaker with Ta CYP20-2 than with At CYP20-2. Increased BZR1 protein levels result in reduced expression of *CPD* during feedback inhibition of BR biosynthesis (Wang et al., 2002). The expression of BR biosynthesis genes, such as *BRASSINOSTEROID-6-OXIDASE*, *CPD*, and *DWARF4*, was lower in transgenic *Arabidopsis* mx3 than the wild type but increased in mx3 *35S:CYP20-2* lines. However, their expressions were more enhanced with At *CYP20-2* compared with Ta *CYP20-2* (see Supplemental Figure 8 online), which suggests feedback regulation of the biosynthesis in the transgenic lines. Therefore, our findings of Ta CYP20-2 as a PPIase with weak activity further suggest that CYP20-2 modulates the conformation of BZR1, which binds to *FLD* to regulate flowering in *Arabidopsis* (Figure 11D).

It is worth noting that CYP20-2 proteins from different species differentially act in GA and BR signaling. In wheat, Ta CYP20-2 is a negative regulator in the GA signaling pathway of DELLA protein degradation (Li et al., 2010a). Ta CYP20-2 interacted with a DELLA protein (RGA) in *Arabidopsis*, but At CYP20-2 did not (Figure 7G). On the other hand, expression of GA biosynthesis genes was altered in the *35S:TaCYP20-2* lines, which may represent a GA signaling response (Xu et al., 1995). The expressions of At *GA20ox1* and At *GA2ox2* were increased in *35S:TaCYP20-2* but not changed in *35S:AtCYP20-2* (Figure 7H). Our conformational analysis suggests that At CYP20-2 has a much stronger and more specific effect on the conformation of BZR1 than does Ta CYP20-2. It is possible that the later flowering of the *35S:TaCYP20-2* lines can be explained by GA signaling that occurs via Ta CYP20-2 interaction with DELLA independent of BZR1. By contrast, the early flowering of *35S:AtCYP20-2* could be mediated by CYP20-2 action on BZR1.

In summary, our studies shed light on BZR1-mediated flowering and help elucidate the protein-level mechanism of CYP-mediated conformational changes in BZR1 to regulate its function. CYP20-2 acts as a molecular chaperone to negatively regulate post-transcriptional modification of BZR1 in *Arabidopsis*. *FLD* is a direct target of BZR1 and mediates the autonomous pathway for flowering.

METHODS

Generation of Transgenic *Arabidopsis* Overexpression Lines

The sequences of genes such as *FLD* and Ta *CYP20-2* were cloned into the pSN1301 vector (modified from vector pCambia1301) (Clontech) containing the CaMV 35S promoter and a β-glucuronidase (*GUS*) gene as a marker. In *pFLD:FLD* (with wild-type BRRE in its promoter) and *pmFLD:FLD* (with the BRRE in its promoter mutated to AGAGAG), the genome sequence of *FLD* with its native promoter was cloned into the vector pCAMBIA1300 (Clontech). At *CYP20-2* was cloned into the pBIN vector (gift from Paul Dupree), which carried a *YFP* gene as a marker. The genes were driven by the CaMV 35S promoter.

Arabidopsis thaliana (Columbia-0 [Col-0]) plants were transformed by the floral dip method (Clough and Bent, 1998). Seeds from *Agrobacterium tumefaciens*–transfected *Arabidopsis* were screened on one-half-strength Murashige and Skoog medium (MS) containing 20 mg/L hygromycin (for OX*FLD*, mx3 *pFLD:FLD*, mx3 *pmFLD:FLD*, and *35S:TaCYP20-2*) or 50 mg/L kanamycin (for *35S:AtCYP20-2*). *Arabidopsis* was grown at 22°C under long-day (16:8 h, light:dark) or short-day (8:16 h, light:dark) conditions.

Quantitative Real-Time PCR

Total RNA was extracted from *Arabidopsis* seedlings with TRNzol A⁺ reagent (Tiangen). cDNA synthesis was performed with Moloney Murine Leukemia Virus Reverse Transcriptase (Promega). For real-time PCR, 2 μg RNA was used for reverse transcription. The cDNA samples were diluted to 2 to 8 ng/mL. Triplicate quantitative assays were performed with 5 μL of each cDNA dilution with the SYBR Green Real-time PCR Master mix (Toyobo) and an MX3000P real-time PCR system (Stratagene). The relative quantification method (Δ-Δ CT) was used to evaluate quantitative variation between the replicates.

Bioinformatics Analysis

Flowering-related genes have been well documented (Fornara et al., 2010). For bioinformatics analysis, Mochiview (Homann and Johnson, 2010) was used to identify putative BZR1-targeted genes, with a BRRE *cis*-element in the promoter (within 1 kb of the transcription start site), and then flowering-related genes were selected from among those putative target genes.

EMSA

EMSA was performed as described (Ma et al., 2009). Briefly, oligonucleotide probes were synthesized, annealed, and labeled by use of the Biotin 3′ End DNA labeling kit (Pierce). *Escherichia coli* BL21 cells transformed with pMAL-ER1-BZR1 and pMAL-C2 plasmids were induced by isopropyl β-D-1-thiogalactopyranoside as described previously. Cells were lysed in lysate buffer (50 mM Tris-HCl, pH 8.0, 1 mM EDTA, and 100 mM NaCl) using an ultrasonic cell crusher. After centrifugation, the supernatant was purified by Amylose Resin affinity chromatography (NEB). The binding reactions were performed according to the manufacturer's protocol. The chemiluminescence of biotin-labeled DNA was detected using the Light Shift Chemiluminescent EMSA kit (Pierce).

ChIP

ChIP experiments were performed as described (Bowler et al., 2004) with 2-week-old plants. Immunoprecipitation was performed with rabbit polyclonal

antibodies against GFP (1:1000) (G1544; Sigma-Aldrich), H3 (1:1000) (17-10046; Millipore), acetylated H3 (1:1000) (17-10241; Millipore), and trimethyl H3K4 (1:300) (17-614; Millipore). Primers and PCR detection of *FLC* regions were as described (Pazhouhandeh et al., 2011). ChIP products were analyzed by quantitative real-time PCR. Data from ChIP experiments are expressed as mean ± SD from three biological replicates.

Protoplast Transient Expression Assay

Isolation of *Arabidopsis* protoplasts was as described (Yoo et al., 2007) with some modifications. The enzyme solution contained 0.3% (w/v) macerozyme R10 (Yakult Pharmaceutical). The isolated protoplasts were transformed with effector, reporter, and reference plasmids at a ratio of 5:3:2 by the polyethylene glycol method. The *pFLD-LUC* reporter gene construct contains the native sequence of the *FLD* promoter fused to luciferase (LUC). *pmFLD-LUC* was generated by replacing CGTGGG in the promoter sequence with AGAGAG. The *BRRE-LUC* reporter gene construct contains a repeat of the BRRE sequence of the *FLD* promoter fused to LUC driven by a mini *35S* promoter. *mBRRE-LUC* was generated by replacing CGTGGG with CATGGG. *35S:GUS* contained a *GUS* gene driven by the CaMV 35S promoter, which was used as an internal control. LUC and GUS enzymatic assays were performed as described (Lin et al., 2007).

Yeast Two-Hybrid Test

Yeast two-hybrid assays for Ta CYP20-2 interaction with At BZR1 and RGA were performed using the Matchmaker system (Clontech). The open reading frames of Ta *CYP20-2* and RGA were inserted in-frame into both pGADT7 and pGBKT7 vectors. Yeast strain AH109 (Clontech) was transformed with pGADT7-TaCYP20-2 and pGBKT7-BZR1, pGADT7-RGA and pGBKT7-TaCYP20-2 plasmids by the lithium acetate–mediated method. Transformants were plated on synthetic dropout selection medium lacking adenine, His, Leu, and Trp. Colonies with a positive signal were examined by activating the lacZ reporter gene.

In Vitro Pull-Down Assay

The fusion proteins from *E. coli DH5α* cells harboring pGEX4T-1-CYP20-2 and pGEX4T-1 plasmids were purified with glutathione Sepharose 4B beads. The beads bound with GST-CYP20-2 and GST were washed with PBS (0.14 M NaCl, 2.7 mM KCl, 10.1 mM Na$_2$HPO$_4$, and 1.8 mM KH$_2$PO$_4$) for GST pull-down assays. Each 300-μL reaction contained total protein (150 μg) from mx3 in 2 mM DTT, 5% glycerol, 1% Triton X-100, and 1 mM phenylmethylsulfonyl fluoride. After being added to glutathione Sepharose 4B beads carrying a GST fusion protein, reaction mixtures were incubated for at least 1 h at 4°C under gentle rotation. After being washed five times with PBS, beads were resuspended with 2× loading buffer (100 mM Tris-HCl, pH 6.8, 200 mM DTT, 4% SDS, 20% glycerol, and 0.2% bromophenol blue). Proteins were eluted at 95°C for 10 min and separated by 12% SDS-PAGE for Coomassie Brilliant Blue staining and immunodetection with anti-GFP antiserum at 1:5000 dilution.

Coimmunoprecipitation Assay

Coimmunoprecipitation assays were performed as described (Zhang et al., 2009) with some modifications. Tobacco (*Nicotiana tabacum*) leaves coexpressing At CYP20-2-YFP and BZR1-FLAG were ground in immunoprecipitation buffer and centrifuged at 20,000*g* for 20 min. Supernatant (1.5 mL) was incubated with anti-GFP coupled to Protein G Sepharose beads overnight under gentle rotation. Beads were washed four times with wash buffer, and the proteins were eluted at 95°C for 10 min in 2×

loading buffer (100 mM Tris-HCl, pH 6.8, 200 mM DTT, 4% SDS, 20% glycerol, and 0.2% bromophenol blue).

Fusion Protein Preparation and PPIase Activity Assay

The cDNA of *CYP20-2* was cloned into the pGEX4T-1 vector to generate pGEX4T-1-*CYP20-2* containing a GST-CYP20-2 fusion construct driven by a lac I promoter. The recombined plasmid was transformed into *E. coli DH5α* cells and grown at 37°C. The GST-CYP20-2 fusion protein was induced by 1 mM isopropyl β-D-1-thiogalactopyranoside for 5 h and purified by glutathione affinity chromatography as described in the Bulk and RediPack GST purification kit (Pharmacia).

PPIase activity assays were performed as described (Fischer et al., 1989). The typical assay mixture consisted of 35 mM HEPES buffer, pH 8.0, 100 μM *N*-succinyl-Ala-Ala-Pro-Phe-*p*-nitroanilide dissolved in 60% (v/v) aqueous dimethyl sulfoxide, 10 μM chymotrypsin, and GST-CYP20-2 or GST at 10 nM. Components of the assay mixture other than chymotrypsin were combined and preincubated at room temperature. Chymotrypsin was added and quickly mixed to initiate the reaction, and absorbance was read at 390 nm every 0.5 s for 2 min with a nucleic acid and protein analyzer (Beckman Coulter DU640).

FTIR

FTIR spectroscopy was performed as described (Li et al., 2009a). The fusion proteins MBP-BZR1, MBP-mBZR1, GST-CYP20-2, MBP, and GST were purified and dissolved in PBS as described previously. PBS was replaced with D$_2$O buffer containing 50 mM K$_2$DPO$_4$/KD$_2$PO$_4$ (pD 7.0) five times using a Microcon YM-3 centrifugal filter unit (Millipore) and Amicon Ultra-0.5 mL, 10-kD Centrifugal Filter Unit (Millipore). The final concentration of MBP-BZR1 and MBP was 12 mg/mL, that of MBP-mBZR1 was 1.25 mg/mL, and that of GST and GST-CYP20-2 was 0.8 mg/mL. FTIR spectra were collected with a spectrometer (ABB-BOMEM; Bureau) equipped with a broadband Mercury-Cadmium-Telluride detector cooled by liquid nitrogen. A two-compartment CaF$_2$ sample cell with a 56-mm-thick Teflon spacer was used for the protein sample and reference D$_2$O or proteins. We collected FTIR for MBP, MBP-BZR1, and MBP-mBZR1 with GST-CYP20-2 or GST in D$_2$O with a volume ratio of 2:1. On average, 50 scans were taken for each spectrum. The assignments of the observed bands in both FTIR and time-resolved IR spectra were performed as described (Ye et al., 2007; Li et al., 2009a).

Isolation of Nucleoprotein and Immunoblot Analysis

Histone-enriched nucleoprotein extraction from 2-week-old *Arabidopsis* seedlings was performed as described (Bowler et al., 2004). The nuclear and cytosolic fractions were separated as described (Gampala et al., 2007). Proteins were analyzed by 15% SDS-PAGE and transferred to polyvinylidene difluoride membranes. Membranes containing the proteins were incubated with antibodies against GFP (1:10,000; G1544; Sigma-Aldrich), H3K4 dimethylation (1:2000), H3K4 trimethylation (1:3000; 17-614; Millipore), H3 acetylation (1:10,000; 17-10241; Millipore), and H3 (1:10,000; 17-10046; Millipore).

Accession Numbers

Sequence data from this article can be found in the Arabidopsis Genome Initiative or GenBank/EMBL databases under the following accession numbers: At *CYP20-2*, At5G13120; *FKBP13*, At5g45680; *FLC*, AT5G10140; *FLD*, AT3G10390; *SOC1*, AT2G45660; *BZR1*, AT1G75080; *CPD*, AT5G05690; *DWF4*, At3g50660; *BR6OX*, AT5G38970; Ta *CYP20-2*, AAP44537; At *GA20o*x1, At4G25420; and At *GA2o*x2, At1G30040. Sequences of PCR primers used in this study are shown in Supplemental Table 2 online.

Supplemental Data

The following materials are available in the online version of this article.

Supplemental Figure 1. Real-Time PCR Analysis of Autonomous Pathway Gene Expression in Col, *35S*:At*CYP20-2* L2 (AOXL2), *35S*: Ta*CYP20-2* (TOXL6), *pBZR1:mBZR1-CFP* (mx3), and *pBZR1:BZR1-CFP* Transgenic *Arabidopsis*.

Supplemental Figure 2. *cyp20-2 fkbp13 cyp40RNAi* Lines Showed Late Flowering.

Supplemental Figure 3. *flc-3* Can Rescue the Late Flowering Phenotype of Overexpression *Ta CYP20-2* Lines.

Supplemental Figure 4. Immunoblot Analysis of Phosphorylation and Unphosphorylation of mBZR1-CFP with or without BL Treatment in mx3.

Supplemental Figure 5. Schematic Diagram to Elaborate the Effect of CYP20-2 on the Secondary Structure of BZR1.

Supplemental Figure 6. Real-Time PCR Analysis of the Expression of *FLD* and *FLC* in *bri1-5* and *bzr1-1D*.

Supplemental Figure 7. *pBZR1:BZR1* Transgenic *Arabidopsis* Did Not Show Obvious Flowering Phenotypes Compared with Col-0.

Supplemental Figure 8. Real-Time PCR Analysis of BR Biosynthetic Genes in mx3, mx3 *35S*:Ta*CYP20-2*, and mx3 *35S*:At*CYP20-2* *Arabidopsis*.

Supplemental Table 1. Putative BZR1-Targeted Flowering-Related Genes.

Supplemental Table 2. Sequences of PCR Oligos Used in This Study.

AUTHOR CONTRIBUTIONS

K.C., Y.X., Y.Z., B.L., and C.Y. designed the research. Y.Z., B.L., D.Z., and S.G. performed the research. K.C., Y.Z., and B.L. analyzed the data. Z.M. performed bioinformatics analysis. Y.W., H.L., and S.L. analyzed the protein secondary structure on FTIR spectroscopy. K.C., Y.Z., Y.X., C.Y., and Y.W. wrote the article.

REFERENCES

Bai, M.Y., Shang, J.X., Oh, E., Fan, M., Bai, Y., Zentella, R., Sun, T.P., and Wang, Z.Y. (2012). Brassinosteroid, gibberellin and phytochrome impinge on a common transcription module in *Arabidopsis*. Nat. Cell Biol. **14:** 810–817.

Bai, M.Y., Zhang, L.Y., Gampala, S.S., Zhu, S.W., Song, W.Y., Chong, K., and Wang, Z.Y. (2007). Functions of OsBZR1 and 14-3-3 proteins in brassinosteroid signaling in rice. Proc. Natl. Acad. Sci. USA **104:** 13839–13844.

Berardini, T.Z., Bollman, K., Sun, H., and Poethig, R.S. (2001). Regulation of vegetative phase change in *Arabidopsis thaliana* by cyclophilin 40. Science **291:** 2405–2407.

Berr, A., Xu, L., Gao, J., Cognat, V., Steinmetz, A., Dong, A., and Shen, W.H. (2009). SET DOMAIN GROUP25 encodes a histone methyltransferase and is involved in *FLOWERING LOCUS C* activation and repression of flowering. Plant Physiol. **151:** 1476–1485.

Bowler, C., Benvenuto, G., Laflamme, P., Molino, D., Probst, A.V., Tariq, M., and Paszkowski, J. (2004). Chromatin techniques for plant cells. Plant J. **39:** 776–789.

Clough, S.J., and Bent, A.F. (1998). Floral dip: A simplified method for Agrobacterium-mediated transformation of *Arabidopsis thaliana*. Plant J. **16:** 735–743.

Clouse, S.D., Langford, M., and McMorris, T.C. (1996). A brassinosteroid-insensitive mutant in *Arabidopsis thaliana* exhibits multiple defects in growth and development. Plant Physiol. **111:** 671–678.

Deng, X., Gu, L., Liu, C., Lu, T., Lu, F., Lu, Z., Cui, P., Pei, Y., Wang, B., Hu, S., and Cao, X. (2010). Arginine methylation mediated by the *Arabidopsis* homolog of PRMT5 is essential for proper pre-mRNA splicing. Proc. Natl. Acad. Sci. USA **107:** 19114–19119.

Domagalska, M.A., Schomburg, F.M., Amasino, R.M., Vierstra, R.D., Nagy, F., and Davis, S.J. (2007). Attenuation of brassinosteroid signaling enhances *FLC* expression and delays flowering. Development **134:** 2841–2850.

Edvardsson, A., Shapiguzov, A., Petersson, U.A., Schröder, W.P., and Vener, A.V. (2007). Immunophilin AtFKBP13 sustains all peptidyl-prolyl isomerase activity in the thylakoid lumen from *Arabidopsis thaliana* deficient in *AtCYP20-2.* Biochemistry **46:** 9432–9442.

Fischer, G., Wittmann-Liebold, B., Lang, K., Kiefhaber, T., and Schmid, F.X. (1989). Cyclophilin and peptidyl-prolyl cis-trans isomerase are probably identical proteins. Nature **337:** 476–478.

Fornara, F., de Montaigu, A., and Coupland, G. (2010). SnapShot: Control of flowering in *Arabidopsis*. Cell **141:** 550.

Gampala, S.S., et al. (2007). An essential role for 14-3-3 proteins in brassinosteroid signal transduction in *Arabidopsis*. Dev. Cell **13:** 177–189.

He, J.X., Gendron, J.M., Sun, Y., Gampala, S.S., Gendron, N., Sun, C.Q., and Wang, Z.Y. (2005). BZR1 is a transcriptional repressor with dual roles in brassinosteroid homeostasis and growth responses. Science **307:** 1634–1638.

He, J.X., Gendron, J.M., Yang, Y., Li, J., and Wang, Z.Y. (2002). The GSK3-like kinase BIN2 phosphorylates and destabilizes BZR1, a positive regulator of the brassinosteroid signaling pathway in *Arabidopsis*. Proc. Natl. Acad. Sci. USA **99:** 10185–10190.

He, Y., Doyle, M.R., and Amasino, R.M. (2004). PAF1-complex-mediated histone methylation of *FLOWERING LOCUS C* chromatin is required for the vernalization-responsive, winter-annual habit in *Arabidopsis*. Genes Dev. **18:** 2774–2784.

He, Y., Michaels, S.D., and Amasino, R.M. (2003). Regulation of flowering time by histone acetylation in *Arabidopsis*. Science **302:** 1751–1754.

Homann, O.R., and Johnson, A.D. (2010). MochiView: Versatile software for genome browsing and DNA motif analysis. BMC Biol. **8:** 49.

Jiang, D., Yang, W., He, Y., and Amasino, R.M. (2007). *Arabidopsis* relatives of the human lysine-specific Demethylase1 repress the expression of *FWA* and *FLOWERING LOCUS C* and thus promote the floral transition. Plant Cell **19:** 2975–2987.

Jin, H., Li, S., and Villegas, A., Jr. (2006). Down-regulation of the 26S proteasome subunit RPN9 inhibits viral systemic transport and alters plant vascular development. Plant Physiol. **142:** 651–661.

Li, B., Xu, W., Xu, Y., Zhang, Y., Wang, T., Bai, Y., Han, C., Zhang, A., Xu, Z., and Chong, K. (2010a). Integrative study on proteomics, molecular physiology, and genetics reveals an accumulation of cyclophilin-like protein, TaCYP20-2, leading to an increase of Rht protein and dwarf in a novel GA-insensitive mutant (*gaid*) in wheat. J. Proteome Res. **9:** 4242–4253.

Li, H., Ke, H., Ren, G., Qiu, X., Weng, Y.X., and Wang, C.C. (2009a). Thermal-induced dissociation and unfolding of homodimeric DsbC revealed by temperature-jump time-resolved infrared spectra. Biophys. J. **97:** 2811–2819.

Li, J., and Jin, H. (2007). Regulation of brassinosteroid signaling. Trends Plant Sci. **12:** 37–41.

Li, J., Li, Y., Chen, S., and An, L. (2010b). Involvement of brassinosteroid signals in the floral-induction network of *Arabidopsis*. J. Exp. Bot. **61:** 4221–4230.

Li, L., Yu, X., Thompson, A., Guo, M., Yoshida, S., Asami, T., Chory, J., and Yin, Y. (2009b). *Arabidopsis MYB30* is a direct target of BES1 and cooperates with BES1 to regulate brassinosteroid-induced gene expression. Plant J. **58:** 275–286.

Li, Q.F., Wang, C., Jiang, L., Li, S., Sun, S.S., and He, J.X. (2012). An interaction between BZR1 and DELLAs mediates direct signaling crosstalk between brassinosteroids and gibberellins in *Arabidopsis*. Sci. Signal. **5:** ra72.

Lim, M.H., Kim, J., Kim, Y.S., Chung, K.S., Seo, Y.H., Lee, I., Kim, J., Hong, C.B., Kim, H.J., and Park, C.M. (2004). A new *Arabidopsis* gene, *FLK*, encodes an RNA binding protein with K homology motifs and regulates flowering time via *FLOWERING LOCUS C*. Plant Cell **16:** 731–740.

Lin, R., Ding, L., Casola, C., Ripoll, D.R., Feschotte, C., and Wang, H. (2007). Transposase-derived transcription factors regulate light signaling in *Arabidopsis*. Science **318:** 1302–1305.

Liu, F., Marquardt, S., Lister, C., Swiezewski, S., and Dean, C. (2010). Targeted 3′ processing of antisense transcripts triggers *Arabidopsis FLC* chromatin silencing. Science **327:** 94–97.

Liu, F., Quesada, V., Crevillén, P., Bäurle, I., Swiezewski, S., and Dean, C. (2007). The *Arabidopsis* RNA-binding protein FCA requires a lysine-specific demethylase 1 homolog to downregulate *FLC*. Mol. Cell **28:** 398–407.

Lu, C., and Armstrong, J.S. (2007). Role of calcium and cyclophilin D in the regulation of mitochondrial permeabilization induced by glutathione depletion. Biochem. Biophys. Res. Commun. **363:** 572–577.

Lu, F., Cui, X., Zhang, S., Jenuwein, T., and Cao, X. (2011). *Arabidopsis* REF6 is a histone H3 lysine 27 demethylase. Nat. Genet. **43:** 715–719.

Luo, X.M., et al. (2010). Integration of light- and brassinosteroid-signaling pathways by a GATA transcription factor in *Arabidopsis*. Dev. Cell **19:** 872–883.

Ma, Q., Dai, X., Xu, Y., Guo, J., Liu, Y., Chen, N., Xiao, J., Zhang, D., Xu, Z., Zhang, X., and Chong, K. (2009). Enhanced tolerance to chilling stress in *OsMYB3R-2* transgenic rice is mediated by alteration in cell cycle and ectopic expression of stress genes. Plant Physiol. **150:** 244–256.

Matouschek, A., Rospert, S., Schmid, K., Glick, B.S., and Schatz, G. (1995). Cyclophilin catalyzes protein folding in yeast mitochondria. Proc. Natl. Acad. Sci. USA **92:** 6319–6323.

Mouradov, A., Cremer, F., and Coupland, G. (2002). Control of flowering time: Interacting pathways as a basis for diversity. Plant Cell **14** (suppl.)**:** S111–S130.

Noh, B., Lee, S.H., Kim, H.J., Yi, G., Shin, E.A., Lee, M., Jung, K.J., Doyle, M.R., Amasino, R.M., and Noh, Y.S. (2004). Divergent roles of a pair of homologous jumonji/zinc-finger-class transcription factor proteins in the regulation of *Arabidopsis* flowering time. Plant Cell **16:** 2601–2613.

Pazhouhandeh, M., Molinier, J., Berr, A., and Genschik, P. (2011). MSI4/FVE interacts with CUL4-DDB1 and a PRC2-like complex to control epigenetic regulation of flowering time in *Arabidopsis*. Proc. Natl. Acad. Sci. USA **108:** 3430–3435.

Rouse, D.T., Sheldon, C.C., Bagnall, D.J., Peacock, W.J., and Dennis, E.S. (2002). FLC, a repressor of flowering, is regulated by genes in different inductive pathways. Plant J. **29:** 183–191.

Ryu, H., Kim, K., Cho, H., and Hwang, I. (2010a). Predominant actions of cytosolic BSU1 and nuclear BIN2 regulate subcellular localization of BES1 in brassinosteroid signaling. Mol. Cells **29:** 291–296.

Ryu, H., Cho, H., Kim, K., and Hwang, I. (2010b). Phosphorylation dependent nucleocytoplasmic shuttling of BES1 is a key regulatory event in brassinosteroid signaling. Mol. Cells **29:** 283–290.

Ryu, H., Kim, K., Cho, H., Park, J., Choe, S., and Hwang, I. (2007). Nucleocytoplasmic shuttling of BZR1 mediated by phosphorylation is essential in *Arabidopsis* brassinosteroid signaling. Plant Cell **19:** 2749–2762.

Searle, I., He, Y., Turck, F., Vincent, C., Fornara, F., Kröber, S., Amasino, R.A., and Coupland, G. (2006). The transcription factor FLC confers a flowering response to vernalization by repressing meristem competence and systemic signaling in *Arabidopsis*. Genes Dev. **20:** 898–912.

Shi, Y., Lan, F., Matson, C., Mulligan, P., Whetstine, J.R., Cole, P.A., Casero, R.A., and Shi, Y. (2004). Histone demethylation mediated by the nuclear amine oxidase homolog LSD1. Cell **119:** 941–953.

Sonmez, C., Bäurle, I., Magusin, A., Dreos, R., Laubinger, S., Weigel, D., and Dean, C. (2011). RNA 3′ processing functions of *Arabidopsis* FCA and FPA limit intergenic transcription. Proc. Natl. Acad. Sci. USA **108:** 8508–8513.

Sun, Y., et al. (2010). Integration of brassinosteroid signal transduction with the transcription network for plant growth regulation in *Arabidopsis*. Dev. Cell **19:** 765–777.

Tang, W., Kim, T.W., Oses-Prieto, J.A., Sun, Y., Deng, Z., Zhu, S., Wang, R., Burlingame, A.L., and Wang, Z.Y. (2008). BSKs mediate signal transduction from the receptor kinase BRI1 in *Arabidopsis*. Science **321:** 557–560.

Tang, W., et al. (2011). PP2A activates brassinosteroid-responsive gene expression and plant growth by dephosphorylating BZR1. Nat. Cell Biol. **13:** 124–131.

Trupkin, S.A., Mora-García, S., and Casal, J.J. (2012). The cyclophilin ROC1 links phytochrome and cryptochrome to brassinosteroid sensitivity. Plant J. **71:** 712–723.

Wang, L., Xu, Y., Zhang, C., Ma, Q., Joo, S.H., Kim, S.K., Xu, Z., and Chong, K. (2008). OsLIC, a novel CCCH-type zinc finger protein with transcription activation, mediates rice architecture via brassinosteroids signaling. PLoS ONE **3:** e3521.

Wang, X., Zhang, Y., Ma, Q., Zhang, Z., Xue, Y., Bao, S., and Chong, K. (2007). SKB1-mediated symmetric dimethylation of histone H4R3 controls flowering time in *Arabidopsis*. EMBO J. **26:** 1934–1941.

Wang, Z.Y., Nakano, T., Gendron, J., He, J., Chen, M., Vafeados, D., Yang, Y., Fujioka, S., Yoshida, S., Asami, T., and Chory, J. (2002). Nuclear-localized BZR1 mediates brassinosteroid-induced growth and feedback suppression of brassinosteroid biosynthesis. Dev. Cell **2:** 505–513.

Xu, Y.L., Li, L., Wu, K., Peeters, A.J., Gage, D.A., and Zeevaart, J.A. (1995). The GA5 locus of *Arabidopsis thaliana* encodes a multifunctional gibberellin 20-oxidase: Molecular cloning and functional expression. Proc. Natl. Acad. Sci. USA **92:** 6640–6644.

Ye, M., Zhang, Q.L., Li, H., Weng, Y.X., Wang, W.C., and Qiu, X.G. (2007). Infrared spectroscopic discrimination between the loop and alpha-helices and determination of the loop diffusion kinetics by

temperature-jump time-resolved infrared spectroscopy for cytochrome c. Biophys. J. **93:** 2756–2766.

Yi, H., Friedman, J.L., and Ferreira, P.A. (2007). The cyclophilin-like domain of Ran-binding protein-2 modulates selectively the activity of the ubiquitin-proteasome system and protein biogenesis. J. Biol. Chem. **282:** 34770–34778.

Yin, Y., Vafeados, D., Tao, Y., Yoshida, S., Asami, T., and Chory, J. (2005). A new class of transcription factors mediates brassinosteroid-regulated gene expression in *Arabidopsis*. Cell **120:** 249–259.

Yin, Y., Wang, Z.Y., Mora-Garcia, S., Li, J., Yoshida, S., Asami, T., and Chory, J. (2002). BES1 accumulates in the nucleus in response to brassinosteroids to regulate gene expression and promote stem elongation. Cell **109:** 181–191.

Yoo, S.D., Cho, Y.H., and Sheen, J. (2007). *Arabidopsis* mesophyll protoplasts: A versatile cell system for transient gene expression analysis. Nat. Protoc. **2:** 1565–1572.

Yu, X., Li, L., Li, L., Guo, M., Chory, J., and Yin, Y. (2008). Modulation of brassinosteroid-regulated gene expression by Jumonji domain-containing proteins ELF6 and REF6 in *Arabidopsis*. Proc. Natl. Acad. Sci. USA **105:** 7618–7623.

Zhang, C., Xu, Y., Guo, S., Zhu, J., Huan, Q., Liu, H., Wang, L., Luo, G., Wang, X., and Chong, K. (2012). Dynamics of brassinosteroid response modulated by negative regulator LIC in rice. PLoS Genet. **8:** e1002686.

Zhang, L.Y., et al. (2009). Antagonistic HLH/bHLH transcription factors mediate brassinosteroid regulation of cell elongation and plant development in rice and *Arabidopsis*. Plant Cell **21:** 3767–3780.

The Cyclophilin CYP20-2 Modulates the Conformation of BRASSINAZOLE-RESISTANT1,
Which Binds the Promoter of *FLOWERING LOCUS D* to Regulate Flowering in *Arabidopsis*

Yuanyuan Zhang, Beibei Li, Yunyuan Xu, Heng Li, Shanshan Li, Dajian Zhang, Zhiwei Mao, Siyi Guo,
Chunhong Yang, Yuxiang Weng and Kang Chong

This information is current as of February 12, 2014